R. & M. No. 2251
(8135)
A.R.C. Technical Report

UNIVERSITY OF MINNESOTA
RECEIVED
SEP
20
1948
LIBRARY

MINISTRY OF SUPPLY

AERONAUTICAL RESEARCH COUNCIL
REPORTS AND MEMORANDA

Pressure Distribution and Wake Traverses on Models of Mustang Wing Section in the Royal Aircraft Establishment and National Physical Laboratory High Speed Tunnels

By

J. S. Thompson, B.A. and M. Markowicz of the R.A.E.
J. A. Beavan, M.A. and R. G. Fowler of the N.P.L.

With Addendum:

Pressure Distribution on a Two-dimensional Mustang Wing Model in the Royal Aircraft Establishment 7-ft. Tunnel

By

J. S. Thompson, B.A. and W. Port

Crown Copyright Reserved

LONDON: HIS MAJESTY'S STATIONERY OFFICE
Price 8*s*. 6*d*. net

Pressure Distribution and Wake Traverses on Models of Mustang Wing Section in the Royal Aircraft Establishment and National Physical Laboratory High Speed Tunnels*

By

J. S. THOMPSON, B.A., and M. MARKOWICZ of the R.A.E.
J. A. BEAVAN, M.A. and R. G. FOWLER of the N.P.L.

COMMUNICATED BY THE PRINCIPAL DIRECTOR OF SCIENTIFIC RESEARCH (AIR), MINISTRY OF SUPPLY

Reports and Memoranda No. 2251

August, 1944

Summary.—Object of Enquiry.—A comparison was required of tests in two high-speed tunnels and in flight.

Range of Investigation.—Pressure distributions and wake traverses were measured for two-dimensional models of Mustang wing section in the Royal Aircraft Establishment and National Physical Laboratory High Speed Wind Tunnels. These readings were taken over an incidence range of about 4 deg. up to the maximum speed of each tunnel.

Conclusions.—The general variations of C_p along the chord and of C_L, C_D and C_M with M agree in the two tunnels, but there is a divergence of absolute values. At low speeds the R.A.E. values of C_p are from 0·05 to 0·10 more negative, the lift curve slope is 10 per cent. greater, and the drag is 40 per cent. higher. The discrepancy in drag is attributed to a rougher model surface and greater tunnel turbulence in the R.A.E. tunnel, giving transition at 0·3c instead of 0·6c in the N.P.L. At high speeds the values of M at which critical changes occur are lower in the R.A.E. tunnel than in the N.P.L., the differences in M being up to 0·04. The comparisons are summarised in Figs. 2 to 10 and 33 to 35.

The aerofoil characteristics are in accordance with its design as a low-drag section, having a $C_D = 0{\cdot}006$ to $0{\cdot}007$ (at $R = 1{\cdot}5 \times 10^6$) prior to a steep shock rise starting at about $M = 0{\cdot}7$. Lift and pitching moment, up to the shock stall, show rises rather greater than predicted by the Glauert formula.

1. *Introduction.*—The object of the experiments described in this report was to obtain a comparison between measurements on similar aerofoils made

(*a*) in flight,

(*b*) in the R.A.E. 10 ft. × 7 ft. High Speed Tunnel,

(*c*) in the N.P.L. 20 in. × 8 in. High Speed Tunnel.

The pressure distribution over the aerofoil surface was measured in each case, and the profile drag was obtained from a pitot traverse of the wake.

This report describes the tests in the two tunnels: the flight results will be issued separately.

2. *Model Particulars.*—Both models were copied from templates of the full-scale wing, which differed considerably from the ideal section. The model ordinates are given in Tables 1 and 2, and the deviations from the ideal section are shown on an exaggerated scale in Fig. 1. The

* R.A.E. Report No. Aero. 1948 received 24th October, 1944.

1520781

N.P.L. model included an irregularity at 0·75 of the chord where the flap hinge was sealed for the full-scale tests. This was not reproduced on the R.A.E. model, but in other respects the two models were nearly identical.

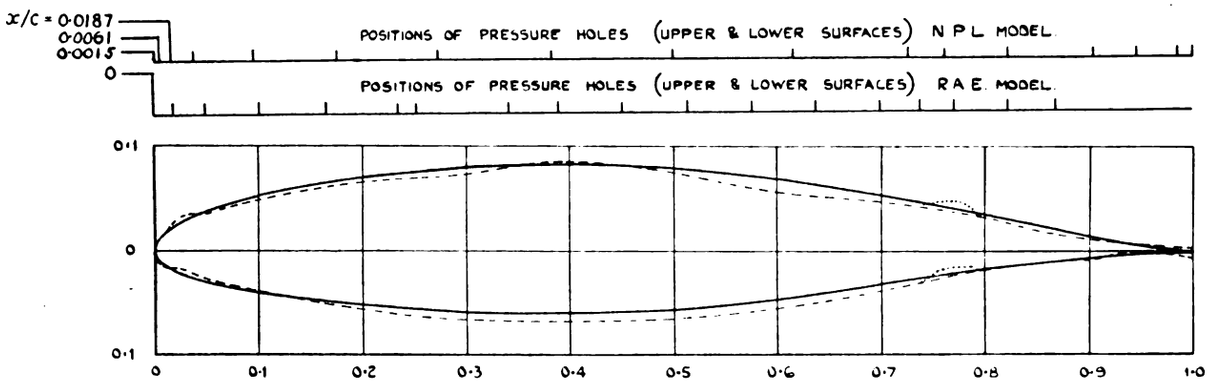

——————— Ideal section (true scale).
- - - - - - - - - - - R.A.E. High Speed Tunnel model (deviations from ideal exaggerated 5 times).
. . . . . N.P.L. High Speed Tunnel model (deviations from ideal exaggerated 5 times).
(N.B.—Where not otherwise shown, N.P.L. and R.A.E. models agree.)

FIG. 1. Mustang Wing Profile and Positions of Pressure Holes.

The leading dimensions are summarised below :—

	R.A.E.	*N.P.L.*
Tunnel height (= aerofoil span)	84 in.	8 in.
Tunnel width	120 in.	17·5 in.
Model chord	24 in.	5 in.
Model thickness/chord	0·145	0·145
Model material	wood	brass
Pressure holes :		
diameter	0·06 in.	0·02 in.
range of spanwise distances from centre line	±1 in.	±2 in.
chordwise positions	*see* Fig. 1	*see* Fig. 1

3. *Method of Test and Analysis.*—(Further details are given in Appendices I and II.)

3.1. *Range.*—The measurements described below were made for a limited incidence range at speeds up to $M = 0{\cdot}8$ in the R.A.E. tunnel and $M = 0{\cdot}83$ in the N.P.L. In the R.A.E. tests the tunnel pressure was adjusted to keep the Reynolds number nearly constant at 2×10^6 ; in the N.P.L. tests the stagnation pressure was constant and the Reynolds number varied from about $1{\cdot}1 \times 10^6$ at $M = 0{\cdot}4$ to $1{\cdot}8 \times 10^6$ at $M = 0{\cdot}8$.

3.2. *Blockage.*—The following corrections were applied to the measured values of M and $\frac{1}{2}\rho V^2$ in the R.A.E. tunnel. These corrections are not quite the same as those given by the latest methods of calculation (Thom[1], 1943) but the differences are not large enough to justify revision of the results.*

M (uncorrected)	0	0·4	0·6	0·7	0·8
$\Delta M/M$	0·005	0·006	0·008	0·011	0·017
$\Delta\frac{1}{2}\rho V^2/\frac{1}{2}\rho V^2$	0·010	0·012	0·016	0·022	0·034

In the N.P.L. tunnel streamlined walls were used according to the usual practice, and no blockage correction was applied.

* Later investigations of blockage corrections (made by testing two-dimensional aerofoils of three different sizes) give experimental values for the corrections which can be applied directly to these tests. On this basis the calculated corrections are slightly too low at the highest speeds, but the differences, which are given in the following table, do not affect any of the main conclusions.

Corrected M as given in this report	0·75	0·78	0·80	0·81
True corrected M	0·751	0·783	0·808	0·823

3.3. *Pressure Distribution.*—The pressure distribution was measured by holes in the surface of the models. A fixed hole in the tunnel wall, upstream of the model, was taken as a datum in each tunnel, and the corresponding free stream pressure was obtained from the known tunnel characteristics.

The coefficients C_L, C_M, C_H have been obtained in the usual way from the areas under C_p curves. The component of pressure along the chord has been neglected, since the cosine of the angle of incidence is nearly unity.

3.4. *Wake Traverses.*—In the R.A.E. wake traverses a pitot comb was used, 0·1 chords aft of the trailing edge, and in the N.P.L. tests a single pitot tube was traversed one chord aft of the trailing edge. The R.A.E. comb was not entirely satisfactory, because the supporting strut influenced the direction of flow at the pitot tubes and made some of the readings low. The comb was calibrated, and a correction has been applied, but the uncertainty of this correction amounts to about $\pm$ 0·0004 in C_D.

The profile drag was calculated by simplified adaptations of the method of Lock, Hilton and Goldstein[2] (1940). In the case of the N.P.L. tests the static pressure correction could be neglected.

4. *Presentation of Results.*—The experimental results are shown in the form of curves, and are classified under the following headings :—

Pressure distribution : C_p, ΔC_p, p/H_0, $M_{\text{crit.}}$

Lift and moment coefficients : C_L, C_M, C_H.

Drag coefficient : C_D.

For a broad comparison of the results, reference should be made to Figs. 2–10, on which R.A.E. and N.P.L. results are plotted together, but fuller details are given on the separate figures for the two tunnels.

A list of the figures is given in the following table, and they are described in more detail below.

Subject	Figure Numbers of Curves showing		
	R.A.E. Results	N.P.L. Results	R.A.E. & N.P.L. Results
Pressure Distribution :—			
C_p *vs* x/c (at constant α) ..	11–14	15–19	2–3
C_p *vs* x/c (at constant C_L) ..			33–35
C_p *vs* M	20–21	22	4–6
p/H_0 *vs* x/c	23	24–25	
ΔC_p *vs* x/c	26	27	
$M_{\text{crit.}}$ *vs* α			7
Lift and Moment Coefficients :—			
C_L *vs* M, α (carpet)			9
C_M *vs* M, α (carpet)	28		
C_M *vs* M		29	
C_{M0} *vs* M			8
C_H *vs* M, α (carpet)		30	
Drag Coefficient :—			
C_D *vs* M	31	32	10
C_D *vs* α		32	

5. *Discussion of Results.*—5.1. *Pressure Distribution.*—The pressure distributions obtained in the two tunnels are compared in Figs. 2 and 3. In each tunnel the distribution on the lower surface is fairly flat at all speeds, but on the upper surface there is a large peak at $x/c = 0 \cdot 4$ and in some cases a smaller one at $x/c = 0 \cdot 2$. These peaks become exaggerated as M increases. Both can be correlated with the deviations from the ideal section shown in Fig. 1. The R.A.E. values of C_p are consistently more negative; this appears both in Figs. 2 and 3, where the results are compared at the same incidence, and in Figs. 33–35 where they are compared at the same C_L.

The variation of C_p with M is shown in Figs. 4–6. The curves approximate to the Kármán law up to $M = M_{\text{crit.}}$; above this speed $-C_p$ rises more steeply in regions where the suction is high. In the forward part of the upper surface $-C_p$ begins to fall when M is slightly greater than $M_{\text{crit.}}$, and towards the trailing edge on both surfaces the suction begins to increase rapidly at a considerably greater value of M. There appears to be a limiting value of the suction corresponding to a local M of about $1 \cdot 3$.

All these effects are common to both tunnels, and the most important difference is that in the R.A.E. tunnel the changes occur at lower values of M. The R.A.E. results also show a slightly higher suction over the whole range.

Fig. 7 shows that the critical speed obtained from the pressure distribution is lower in the R.A.E. tunnel.

5.2. *Coefficients C_L and C_M.*—The lift carpets obtained in the two tunnels are shown in Fig. 9. As M increases, C_L shows the usual gradual rise followed by a sharp fall, but in the R.A.E. tests the fall occurs earlier and more steeply than in the N.P.L. tests. Fig. 9 also shows another serious difference between the tunnels in the slope of the lift curve, which is 10 per cent. higher in the R.A.E. tests over all the low speed range.*

Pitching moments can best be compared on the C_{M0} curves in Fig. 8. The R.A.E. values are lower throughout, and the minimum value occurs at a lower speed in the R.A.E. tunnel than in the N.P.L.

5.3. *Drag.*—The drag coefficients are compared for $\alpha = 0$ in Fig. 10. The R.A.E. values are considerably larger at low speeds, but the tunnels agree in showing a steep rise between $M = 0 \cdot 7$ and $0 \cdot 8$.

6. *Conclusions.*—6.1. *Comparison of Results in the Two Tunnels.*—There seem two major classes of difference between the two tunnels.

6.11. *Low speed.*—At low speeds :—

R.A.E. C_p is $0 \cdot 05$ to $0 \cdot 1$ more negative.
R.A.E. Lift curve slope is 10 per cent. higher.*
R.A.E. C_{M0} is $0 \cdot 005$ more negative.
R.A.E. C_D is $0 \cdot 003$ higher.

The most obvious differences in the conditions of test were :—

(1) R.A.E. tunnel may be more turbulent.
(2) R.A.E. model had a less smooth finish.

Either of these factors could account for the discrepancy in C_D, which indicates a very much further back transition in the N.P.L. tests. In this case some part of the difference in the other coefficients may also be explained. (Large variations, both positive and negative, have been found in other tunnels at low M, with change of transition point.)

(3) The R.A.E. tunnel walls were straight, and those of the N.P.L. were streamlined. However, the tunnel constraint correction required to make the results agree is greater than would be expected at low speeds.

* *See* Addendum for further tests and discussion of this point.

(4) R.A.E. has a better span/chord ratio (3·5 instead of 1·6). However, according to Preston[5] (1944), the measured boundary layer of the N.P.L. tunnel should not have reduced the lift slope by more than 2–3 per cent.

(5) In the R.A.E. model only the middle nine inches of the span was of the true section (Appendix I).

(6) On the N.P.L. model the pressure holes were widely spaced along the span (Appendix II).

6.12. *High speed.*—The correspondence between the values of M at the upper end of the range, at which critical events occur, as distinct from differences in the coefficients at lower speeds as in sect. 6.11 above, is very roughly

R.A.E.:	$M = 0{\cdot}64$	0·70	0·75	0·78
N.P.L.:	$M = 0{\cdot}65$	0·72	0·78	0·82

To reconcile the results the R.A.E. values would require an additional blockage correction very much larger than seems probable. Measurements of the pressures on the tunnel walls suggest, however, that the R.A.E. blockage corrections may be too small at high speeds, and since the method of streamlining used in the N.P.L. applies a considerable part of the correction automatically the N.P.L. results are more likely to be correct. Further analysis is being made of these and other wall pressure measurements, which it is hoped will clarify matters. Both R.A.E. and N.P.L. corrections are derived from the theory of images, and there is some doubt as to the validity of this method at high speeds when shock waves are present.*

6.2. *High Speed Characteristics of the Aerofoil.*—6.21. *Low drag before the shock rise.*—The aerofoil was designed semi-empirically in the U.S.A. to give low drag, the ideal section having a fairly small negative pressure gradient over the leading 50–60 per cent. of both surfaces at ordinary high speed incidence.

The actual sections tested showed this gradient, with minor irregularities, up to the critical speed, and the N.P.L. measurements of C_D prove that in fact transition is kept far back over the whole of the lower range of M and for incidence $-$ 1 deg. to $+$ 1 deg.

6.22. *Shock rise of drag.*—At a speed somewhat above the critical ($M = 0{\cdot}67$ at $\alpha = 0$ deg.) the drag increases rapidly as follows.

Increase on low speed value	30 per cent.	100 per cent.	500 per cent.
M	0·71	0·735	0·78

Recent measurements (unpublished) on the same wing section on a Mustang aircraft in flight have shown comparable results. In particular, the flight tests show an equally rapid rise of drag with Mach number.

6.23. *Shock wave position.*—When sonic speeds are reached on the aerofoil, the small upraising of the pressure distribution on the upper surface, at from 35–50 per cent. of the chord, becomes greatly intensified and then forms the supersonic region of which the shock wave makes the rear. Until the speed is much higher, this shock wave moves back only slowly.

6.24. *Effect of surface Irregularities at 75 per cent. chord.*—The pronounced kinks in the N.P.L. pressure distributions at about 75 per cent. chord, due to surface bumps, are unimportant. They cannot have brought about breakaway before $M = 0{\cdot}7$ approx. since low drag was obtained up to that speed.

6.25. *Variation of lift with M.*—As with more conventional aerofoils C_L rises slowly with M up to the compressibility stall, which for $\alpha = 0{\cdot}5$ deg. occurs at a value of M 0·05 greater than the critical. The delay in the stall is greater at smaller incidence, probably because then the critical is soon reached on the lower surface as well, and the breakdown of suction behind the shock wave there gives a counter balance to that already in progress on the upper surface.

Prior to the shock stall, a_1 rises more steeply than Glauert's formula, and would probably agree better with Kármán's modified form. This was not calculated since theoretical pressure curves were not available.

---

* *See* footnote to section 3.2 page 2.

6.26. *Variation of pitching moment with Mach number.*—The pitching moment compressibility stall occurs a little later than that for the lift and is more violent. The rate of increase is again greater than by Glauert's formula.

Hilton's empirical law[6] (1943) for C_{M0}, with an assumed low-speed value, gives reasonable agreement with the results, up to the compressibility stall.

6.27. *Hinge moment.*—The sample calculation of the moment of the tail quarter-chord, giving a rough value of C_H for a 25 per cent. control in its neutral position, shows a numerical increase of the negative values with increase of speed. The compressibility stall is violent.

6.3. *Comparison with Flight Results.*—One C_p curve obtained in flight has been plotted in Fig. 35. No definite conclusions can be drawn until the complete results are available.*

6.4. *Further Work.*—(1) Theoretical pressures for the actual sections used will be calculated by Goldstein's methods, if possible, as a guide to discriminating between the results in the two tunnels.

(2) It is suggested that a further section already thoroughly tested at the N.P.L., and designed to a theoretical distribution by Goldstein, be tested at the R.A.E.

(3) Measurements on the effect of Reynolds number and tunnel constraint on drag measurement are being made in the R.A.E. tunnel.

NOTATION

H_0	free stream total head
H	local total head
p_0	free steam static pressure
p	local static pressure
C_p	$(p - p_0)/\frac{1}{2}\rho V^2$
C_{p0}	value of C_p at $M = 0$ from von Kármán's law
ΔC_p	C_p on upper surface $-$ C_p on lower surface
$(C_p)_{\text{crit.}}$	value of C_p at which local $M = 1$
$M_{\text{crit.}}$	free stream Mach number for which C_p reaches $(C_p)_{\text{crit.}}$ at some point on the surface
C_H	(hinge moment of area aft of $0{\cdot}75c)/\frac{1}{2}\rho V^2\, b(\frac{1}{4}c)^2$ where b = span
x	distance along chord from leading edge
y	perpendicular distance from chord line, positive towards upper surface
z	$\frac{1}{2}(x/c - \frac{1}{4})^2$
$\cos\theta$	$1 - 2x/c$
W, η, δ	wake parameters : *see* Fig. 37.

von Kármán's law $\dfrac{1}{C_p} - \frac{1}{2} = \left(\dfrac{1}{C_{p0}} - \frac{1}{2}\right)\sqrt{(1 - M^2)}$

a_1	$dC_L/d\alpha$
b_1	$dC_H/d\alpha$

---

* Later flight results show reasonably good agreement over the whole speed range.

REFERENCES

No.	Author	Title, etc.
1	A. Thom	Blockage Corrections in a Closed High Speed Tunnel. R. & M. 2033. November, 1943.
2	C. N. H. Lock, W. F. Hilton and S. Goldstein	Determination of Profile Drag at High Speeds by a Pitot Traverse Method. R. & M. 1971. September, 1940.
3	H. B. Squire and A. D. Young	The Calculation of the Profile Drag of Aerofoils. R. & M. 1838. November, 1937.
4	N. E. Winterbottom and H. B. Squire ..	Note on Further Wing Profile Drag Calculations. R.A.E. Report B.A. 1634. A.R.C. 4871. October, 1940. Addendum to R. & M. 1838.
5	J. H. Preston	The Interference on a Wing Spanning a Closed Tunnel arising from Boundary Layers on the Side Walls, with Special Reference to the Design of Two-dimensional Tunnels. R. & M. 1924. March, 1944.
6	W. F. Hilton	Empirical Laws for the Effect of Compressibility on Quarter-chord Moment Coefficient, and for the Choice of an Aerofoil with Small Compressibility Effects on Centre of Pressure R. & M. 2195. March, 1943.
7	W. F. Davis	Comparison of Various Methods of computing Drag from Wake Surveys. N.A.C.A. Advance Restricted Report. January, 1943. A.R.C. 6679.
8	J. A. Beavan and G. A. M. Hyde	Compressibility Increase of Lift and Moment on EC 1250 for Low Speed $C_L = 0 \cdot 17$. R. & M. 2055. September, 1942.
9	C. N. H. Lock and J. A. Beavan	Tunnel Interference at Compressibility Speeds using the Flexible Walls of the Rectangular High Speed Tunnel. R. & M. 2005. September, 1944.
10	J. A. Beavan	Note on Methods at the N.P.L. and in the U.S.A. for calculating the Profile Drag at High Speeds from Pitot Traverse Measurements. R. & M. 2102. April, 1943.

References for the Addendum are on page 44.

APPENDIX I

Details of Royal Aircraft Establishment Tests

Model.—The model was of wood, and the pressure holes were made with $\frac{1}{16}$ in. bore copper pipe, the ends of the pipe being filed flush with the wing surface. This method is not entirely satisfactory, but it is not believed to cause any systematic errors.

The aerofoil was originally made to the ideal section, and only the middle nine inches of the span were altered when it was decided to copy the full scale templates.

Pressure Measurements.—The tunnel speed was obtained in the usual way from the pressures at two reference holes in the tunnel wall, one in the settling chamber (R), and the other just ahead of the working section (C). These measurements, with a previous tunnel calibration, gave the speed and static pressure in the working section. Pressure differences between the C hole and the holes in the aerofoil surface were measured with alcohol manometers.

Lift and pitching moment coefficients were obtained by taking the pressure differences ΔC_p between corresponding holes in the upper and lower surfaces, and integrating curves of ΔC_p against x/c for C_L and against $\frac{1}{2}(x/c)^2 - \frac{1}{4}(x/c)$ for C_M.

Wake Drag Measurements.—The total head measurements in the wake were made with alcohol manometers, using the reference hole R in the settling chamber as a common datum. The free stream total head was obtained from the tunnel calibration, or from the end tubes of the comb when they were clear of the wake.

The drag was calculated from the area under the loss curve $(H_0 - H)/(H_0 - p_0)$ against y/c, using a factor F_c to convert this to C_D, where F_c is a function of M, $(p - p_0)/(H_0 - p_0)$ in the wake, and η, the maximum value of $(H_0 - H)/(H_0 - p_0)$ in the wake. The method is similar to one described by Davis[7] (1943) but Fig. 5 in that report contains serious errors and was not used.

The pitot comb was about $0 \cdot 3c$ long, but at speeds greater than about $M = 0 \cdot 7$ the wake extended beyond it at the upper surface end. A few typical wake traverses are given in Fig. 36, and other details of the wake in Fig. 37.

APPENDIX II

Details of National Physical Laboratory Tests

1. *Further Details of the Model.*—The 34 pressure holes were drilled within the middle 4 in. of the 8 in. span, being distributed in a fairly random arrangement, as follows :—

Hole number	1	2	3	4	5	6	7	8	9
x/c	0	0·0016	0·0062	0·0188	0·038	0·096	0·175	0·273	0·383
Distance from mid tunnel (in). U.S.	+0·3	−0·5	+0·7	−0·9	−1·3	−1·9	+1·7	−1·5	−0·1
Distance from mid tunnel (in). L.S.		−0·3	+1·3	−0·7	−1·1	+1·5	−1·7	+1·9	+1·1

10	11	12	13	14	15	16	17	18
0·500	0·617	0·727	0·761	0·825	0·905	0·946	0·986	1·000
+1·7	−1·5	−0·3	−1·9	+0·9	−1·7	+0·1	−0·9	−0·1
+1·5	+1·9	−1·1	−0·7	+1·3	−1·3	+0·5	−0·5	

2. *Range of Test.*—(1) The original pressure plotting covered the following range :—

Incidence : ± 2 deg., ± 1 deg. and 0 deg. (Tests at ± 3 deg., + 4 deg., + 5 deg. have not been computed.)

Speed : $M = 0{\cdot}3$ to $0{\cdot}85$. The tunnel walls were set "streamline"[8,9] for each of the speeds $M = 0{\cdot}57$, $0{\cdot}68$, $0{\cdot}73$, $0{\cdot}78$, $0{\cdot}83$, $0{\cdot}88$ and tests were made for a range of speed at each setting. Fig. 38 is an example of the final results, with these ranges distinguished.

(2) After the above tests had been made and the results reduced, a twist in the flow was discovered, caused by the copper gauzes around the intake. The swirl, amounting to ± 0·5 deg. variation of pitch across the middle 4 in. of the span, was eliminated by fitting straighteners, and a number of repeat readings at ± 2 deg. and 0 deg. were taken.

The pressure distribution over the nose was considerably smoothed by this correction while the only other hole affected was that at $x/c = 0{\cdot}617$ on the upper surface. The consequent change in C_L was small, but C_M was reduced in magnitude although its variation with M remained similar (Fig. 38).

The results presented are all for corrected wind direction, but interpolation was sometimes necessary, using the previous results as a guide.

(3) The wake traverses to find the drag were made over the following ranges :—

(*a*) At 0 deg. and ± 1 deg., from $M = 0{\cdot}4$ to $0{\cdot}8$,

(*b*) At $M = 0{\cdot}46$ and $0{\cdot}57$, angle ranges − 3 deg. to + 5 deg.

3. *Experimental Technique.*—The pressure readings were taken on a multi-tube mercury manometer with reservoir backed by the total head in the intake, behind the gauzes. Tunnel speed was measured by the pressure at a hole in the wall 1·7 chords ahead of the aerofoil leading

edge on the upper surface side. The speed at this point never differed from that on the opposite side of the tunnel by as much as 1 per cent. In the empty tunnel the speed at these wall holes agreed to within $\frac{1}{2}$ per cent. with that at the middle, the static distribution across the tunnel being very nearly uniform.

The traverses for drag measurement were made one chord behind the aerofoil, where the static pressure variation due to the aerofoil could be neglected.

4. *Reduction of the Observations.*—The standard N.P.L. High Speed Tunnel method of plotting pressures first on a basis of $\theta = \cos^{-1}(1 - 2x/c)$ was followed. Use of this parameter provides an enlarged scale around the nose so that the observations can be plotted more smoothly through that region. The ordinary pressure distribution curve against x/c and a pitching moment curve on a basis of $z = \frac{1}{2}(x/c - \frac{1}{4})^2$ were then derived from the master θ curve by using superimposed transparent grids which had rulings at even values of x/c and z respectively. (Form drag could be obtained similarly from the same θ curves.)

The resulting curves are directly integrable to give the lift and pitching moment about the quarter-chord. Two examples of the process are shown on a reduced scale in Fig. 39.

For the " hinge moment " C_H of the tail about the three-quarter chord point, no refinement was thought necessary on the very approximate but quick method of summing the products of the pressure difference between the surfaces at $x/c = 0{\cdot}8$, $0{\cdot}85$, $0{\cdot}9$ and $0{\cdot}95$ and the respective distances of these points from $0{\cdot}75c$.

The calculation of C_{D0} from the wake traverses was carried out using the very much simplified formula (3) of Ref. 10.

TABLE 1

Mustang Wing Ordinates

Distance from Leading Edge	Ideal Section		R.A.E. Model (24 in. Chord)		*N.P.L. Model (5 in. Chord)	
	Upper Surface	Lower Surface	Upper Surface	Lower Surface	Upper Surface	Lower Surface
0	0	0	0	0	0	0
1·25	1·91	1·63	1·92	1·65	1·94	1·66
2·50	2·68	2·24	2·77	2·19	2·75	2·18
5·00	3·80	3·01	3·75	2·94	3·78	2·94
7·50	4·59	3·57	4·56	3·50	4·54	3·51
10·0	5·26	4·02	5·19	4·00	5·15	3·99
15·0	6·33	4·68	6·25	4·73	6·20	4·72
20	7·06	5·18	6·94	5·30	6·95	5·29
25	7·62	5·56	7·50	5·67	7·51	5·68
30	8·07	5·79	7·94	5·94	7·93	5·94
40	8·43	5·93	8·46	6·09	8·44	6·08
50	8·00	5·59	7·91	5·77	7·93	5·77
60	6·95	4·57	6·75	4·73	6·71	4·74
70	5·45	3·11	5·31	3·29	5·31	3·30
80	3·56	1·73	3·50	1·75	3·52	1·72
90	1·46	0·55	1·42	0·58	1·40	0·61
95	0·61	0·21	0·65	0·19	0·66	0·16
100	0	0	0·08	0·12	0·07	0·12

All distances are expressed as percentage of the chord.

* Further details of N.P.L. ordinates are given in Table 2.

TABLE 2

N.P.L. Test Section

Distance along Chord from Leading Edge. Inches	Above Chord. Inches	Below Chord. Inches	Distance along Chord from Leading Edge. Inches	Above Chord. Inches	Below Chord. Inches
0	0	0	2·3	0·4120	0·2980
0·005	0·0278	0·0265	2·4	0·4055	0·2940
0·010	0·0393	0·0369	2·5	0·3965	0·2885
0·015	0·0483	0·0446	2·6	0·3865	0·2805
0·020	0·0557	0·0509	2·7	0·3750	0·2715
0·025	0·0623	0·0562	2·8	0·3620	0·2615
0·030	0·0683	0·0610	2·9	0·3495	0·2495
0·035	0·0737	0·0653	3·0	0·3355	0·2370
0·040	0·0790	0·0692	3·1	0·3225	0·2235
0·050	0·0875	0·0755	3·2	0·3085	0·2100
0·060	0·0950	0·0815	3·3	0·2945	0·1955
0·070	0·1025	0·0865	3·4	0·2805	0·1805
0·080	0·1095	0·0915	3·5	0·2655	0·1650
0·090	0·1165	0·0960	3·6	0·2505	0·1485
0·100	0·1230	0·1000	3·65	0·2425	0·1400
0·125	0·1375	0·1090	3·675	0·2385	0·1355
0·150	0·1500	0·1180	3·700	0·2345	0·1310
0·175	0·1610	0·1260	3·725	0·2310	0·1260
0·200	0·1710	0·1335	3·750	0·2275	0·1175
0·250	0·1890	0·1470	3·775	0·2235	0·1130
0·300	0·2050	0·1590	3·800	0·2205	0·1095
0·350	0·2200	0·1705	3·825	0·2170	0·1065
0·400	0·2340	0·1805	3·850	0·2130	0·1035
0·450	0·2460	0·1900	3·875	0·2090	0·1005
0·500	0·2575	0·1995	3·900	0·2035	0·0975
0·600	0·2805	0·2150	3·925	0·1960	0·0945
0·700	0·3010	0·2295	3·950	0·1875	0·0915
0·80	0·3190	0·2425	3·975	0·1815	0·0890
0·90	0·3340	0·2545	4·0	0·1760	0·0860
1·0	0·3475	0·2645	4·1	0·1530	0·0750
1·1	0·3595	0·2730	4·2	0·1305	0·0635
1·2	0·3705	0·2805	4·3	0·1090	0·0530
1·3	0·3800	0·2870	4·4	0·0890	0·0415
1·4	0·3890	0·2925	4·5	0·0700	0·0305
1·5	0·3965	0·2970	4·6	0·0545	0·0195
1·6	0·4050	0·3005	4·7	0·0400	0·0110
1·7	0·4120	0·3030	4·75	0·0330	0·0080
1·8	0·4175	0·3040	4·8	0·0265	0·0080
1·9	0·4210	0·3045	4·85	0·0205	0·0080
2·0	0·4220	0·3040	4·9	0·0145	0·0080
2·1	0·4205	0·3030	4·95	0·0090	0·0075
2·2	0·4170	0·3010	5·0	0·0035	0·0060

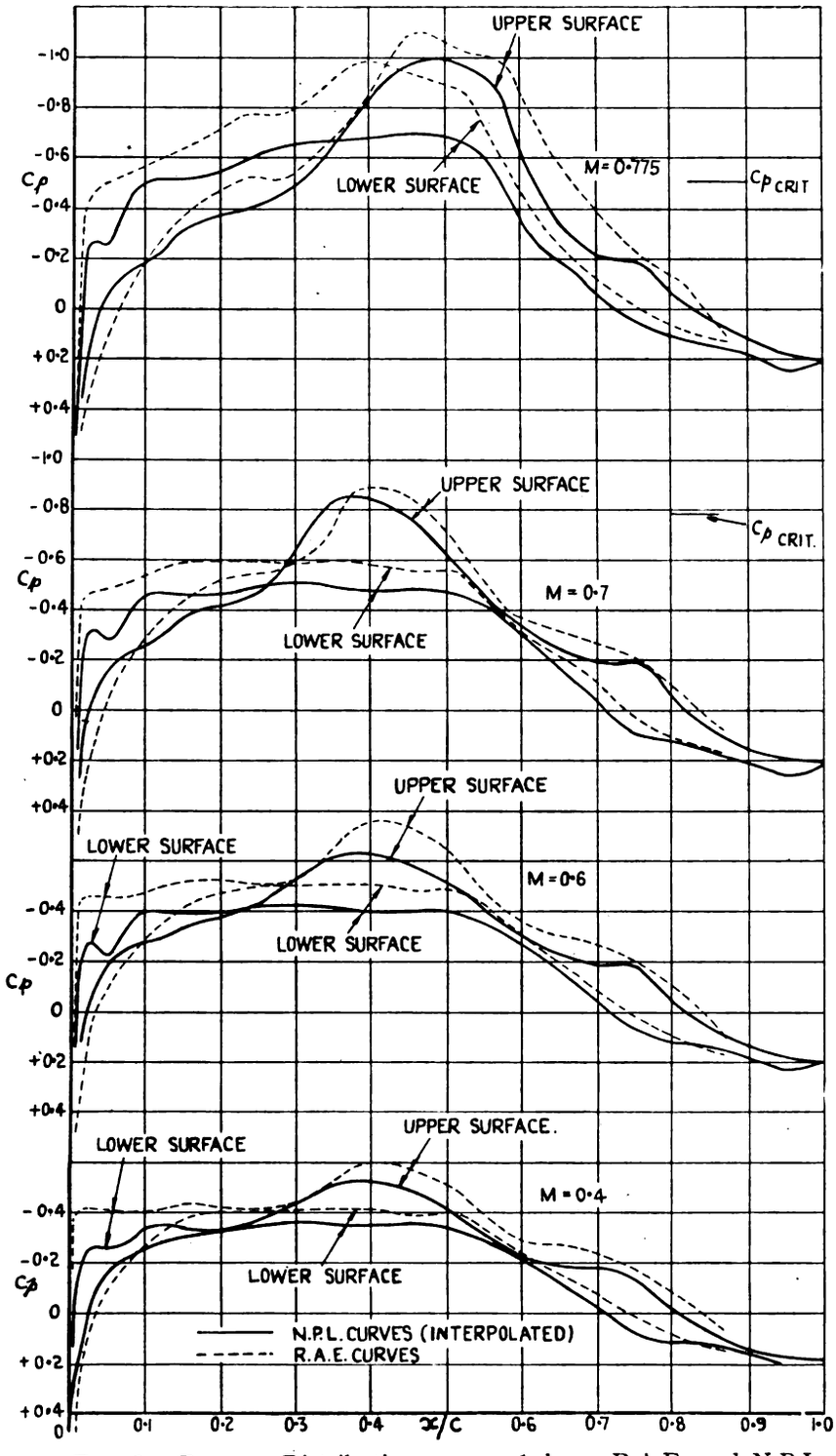

FIG. 2. Pressure Distribution, $\alpha = -1$ deg. R.A.E. and N.P.L. High Speed Tunnels.

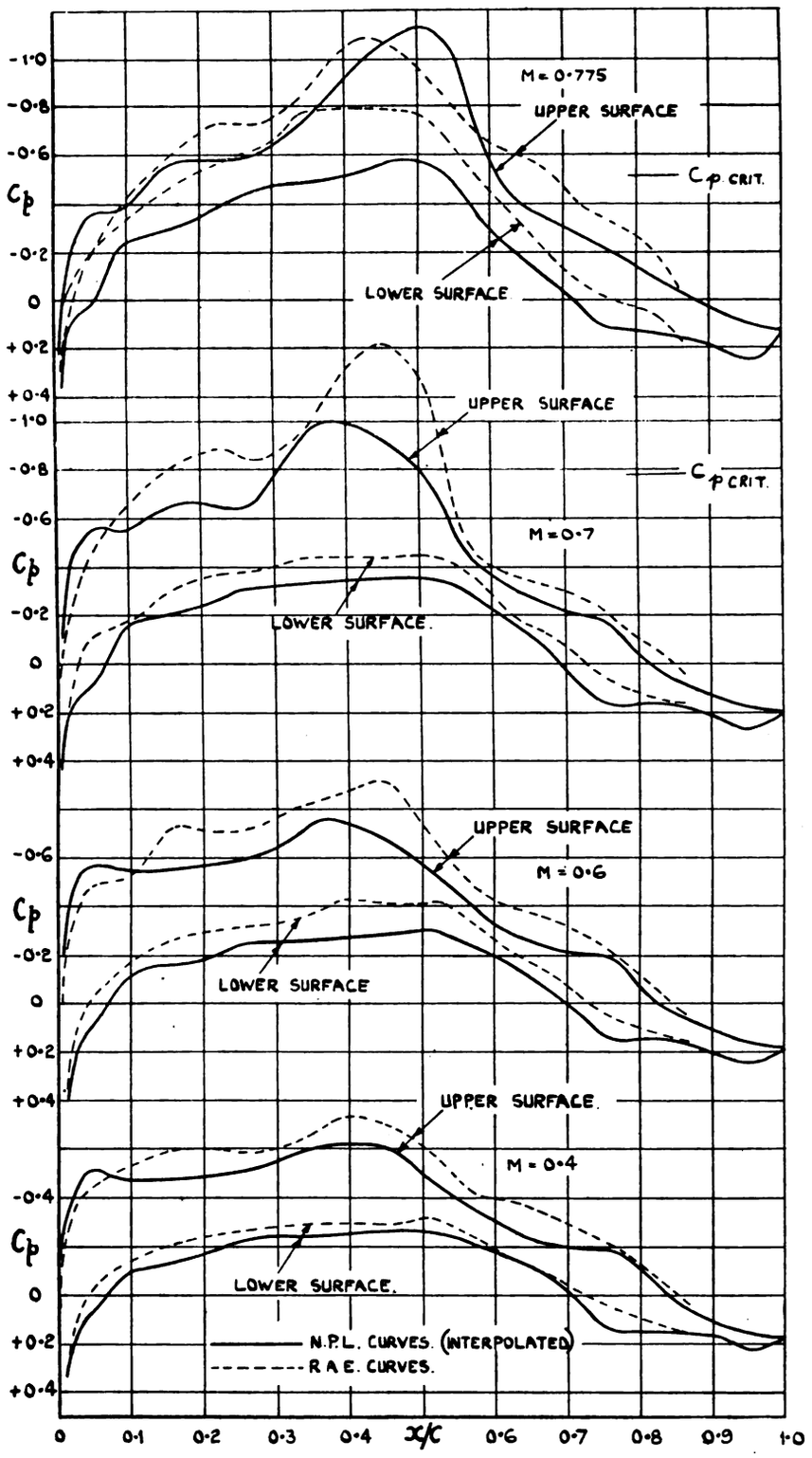

FIG. 3. Pressure Distribution. $\alpha = +1$ deg. R.A.E. and N.P.L. High Speed Tunnels.

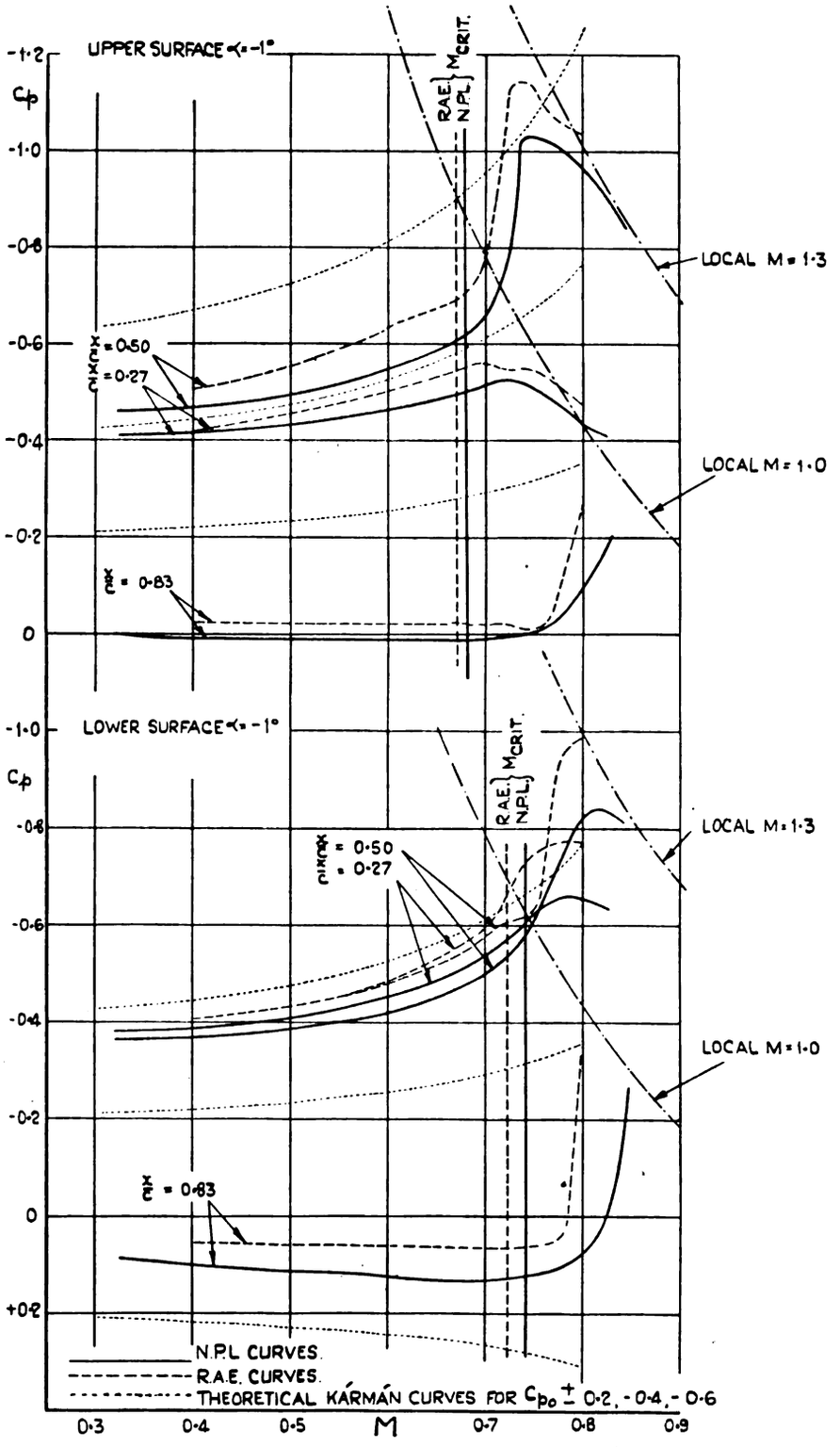

FIG. 4. Variation of C_p with M. $\alpha = -1$ deg. R.A.E. and N.P.L. High Speed Tunnels.

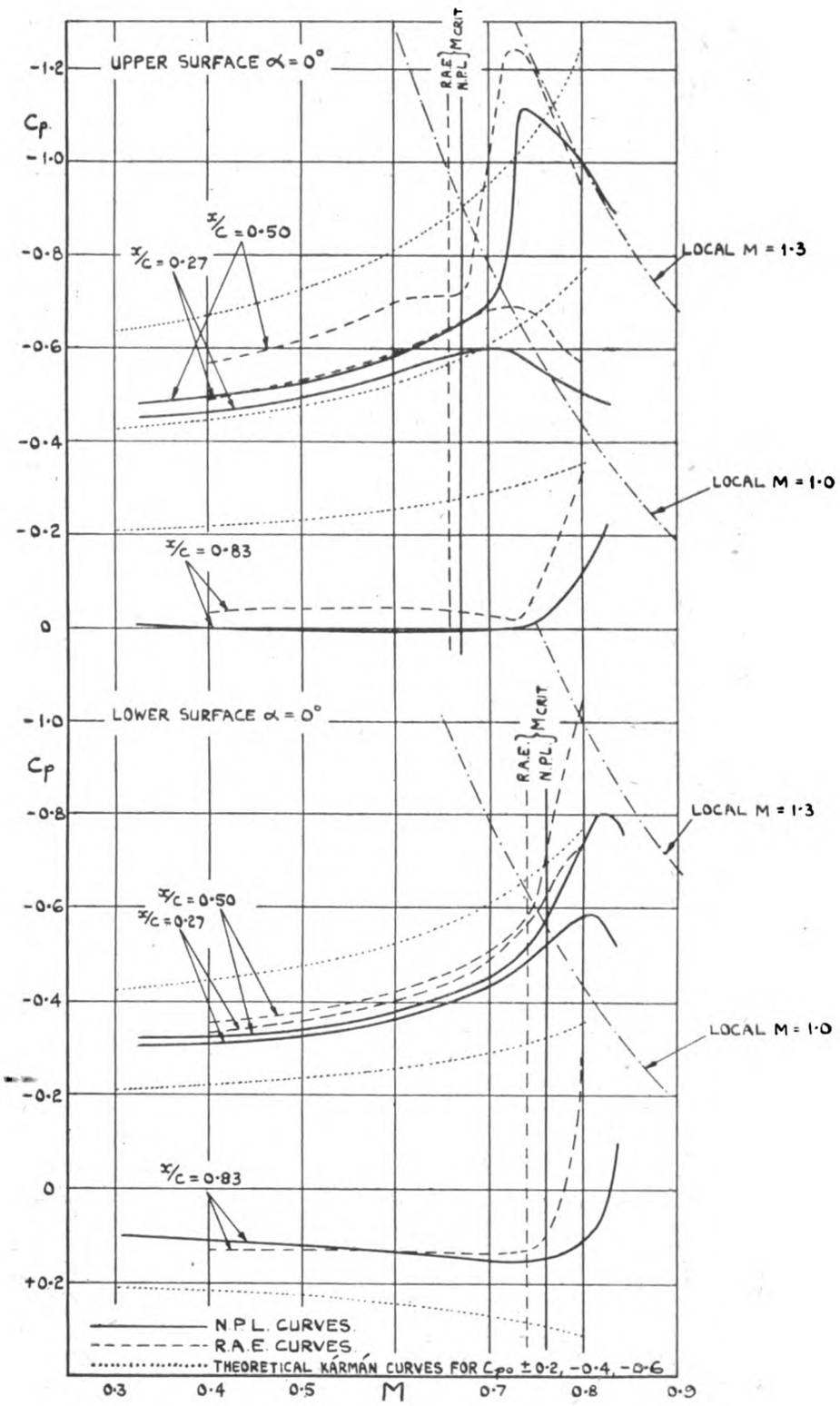

FIG. 5. Variation of C_p with M. $\alpha = 0$ deg. R.A.E. and N.P.L. High Speed Tunnels.

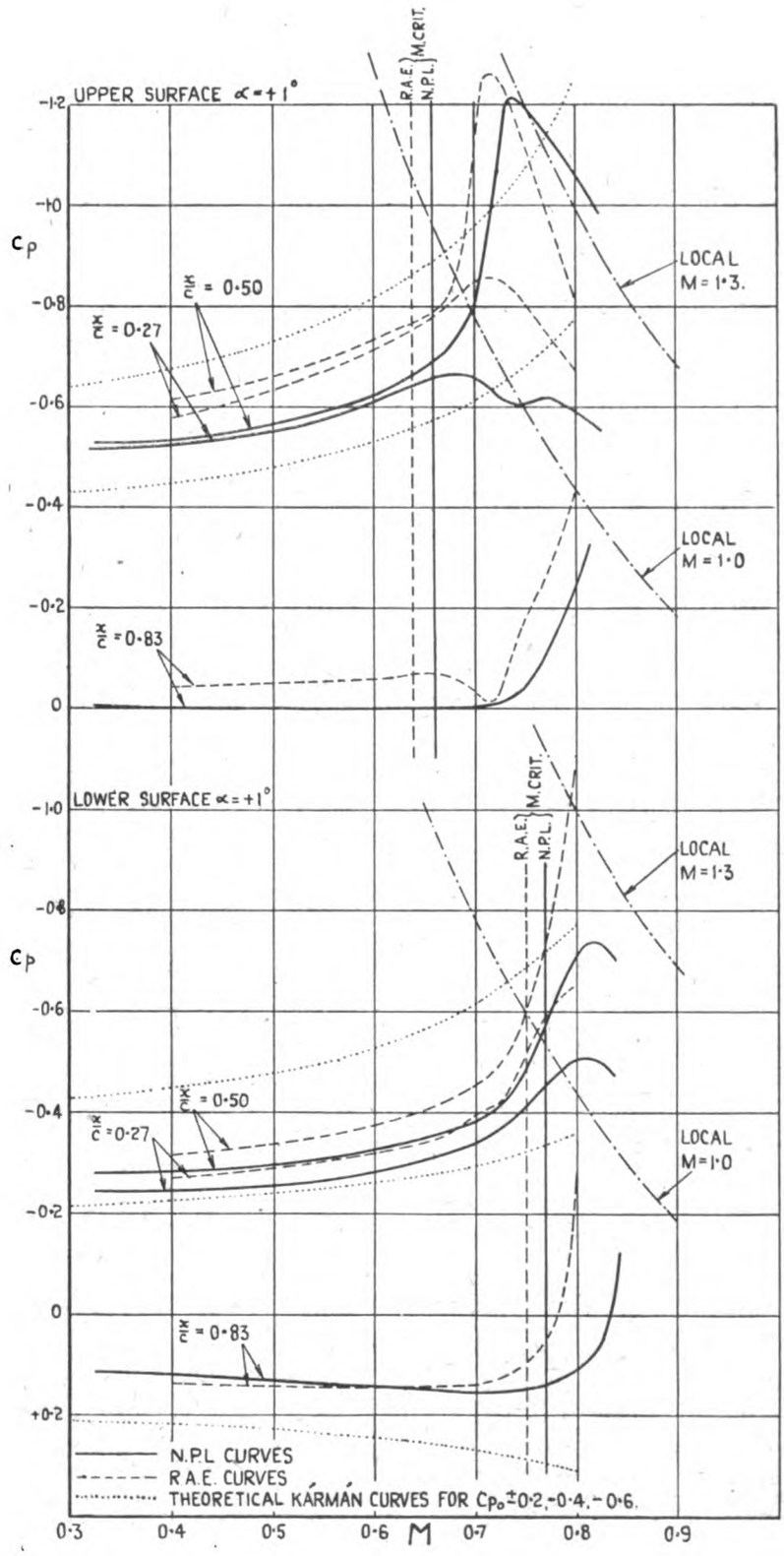

FIG. 6. Variation of C_p with M. $\alpha = +1$ deg. R.A.E. and N.P.L. High Speed Tunnels.

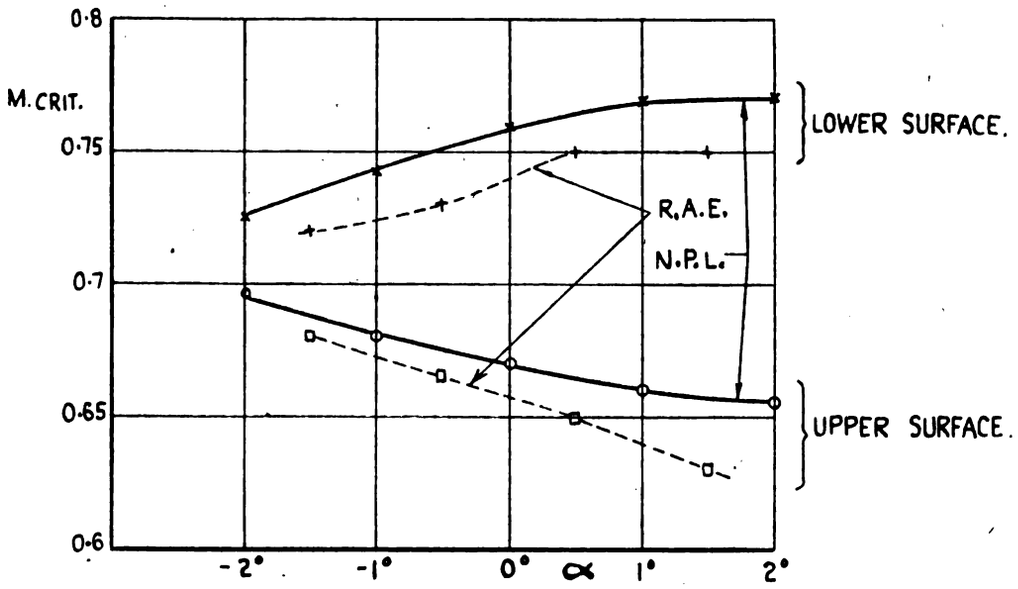

FIG. 7. Comparison of Critical Mach Number.

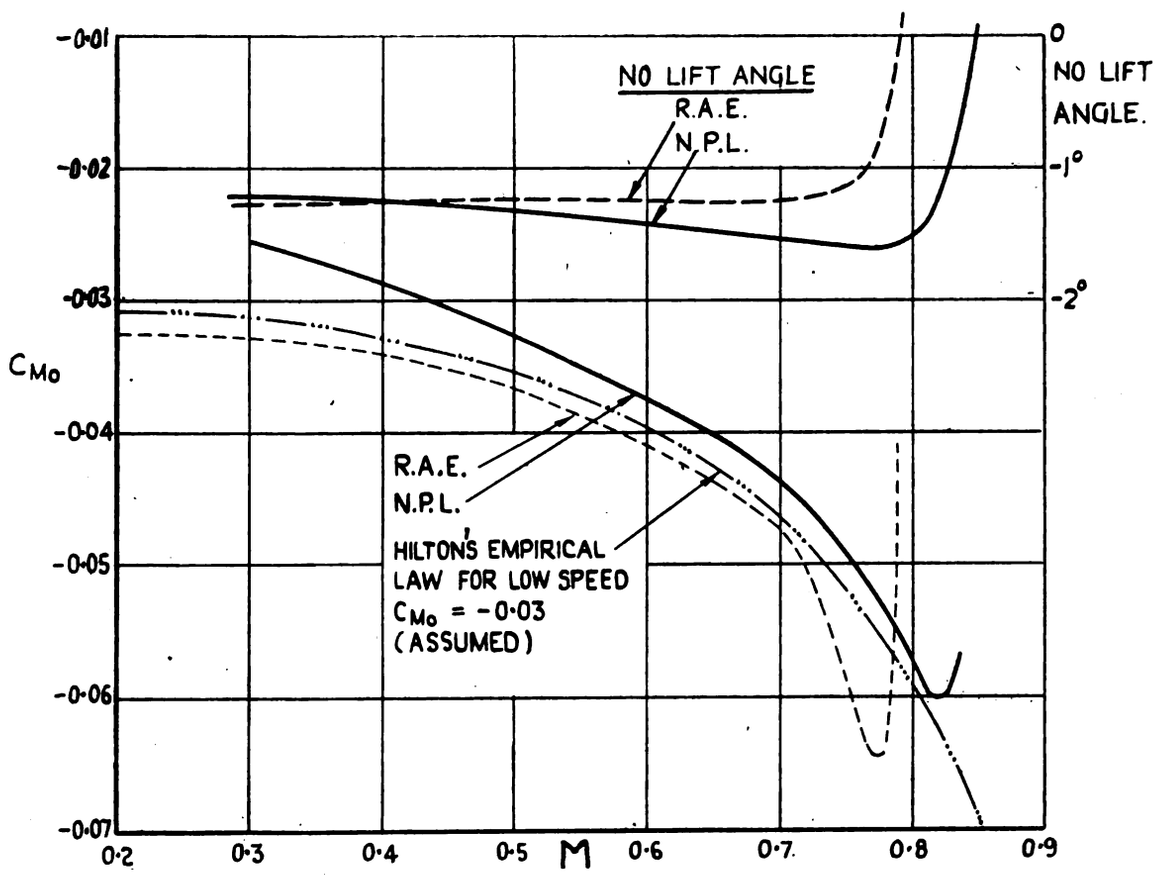

FIG. 8. Variation of C_{M0} and No-Lift Angle with M. R.A.E. and N.P.L. High Speed Tunnels.

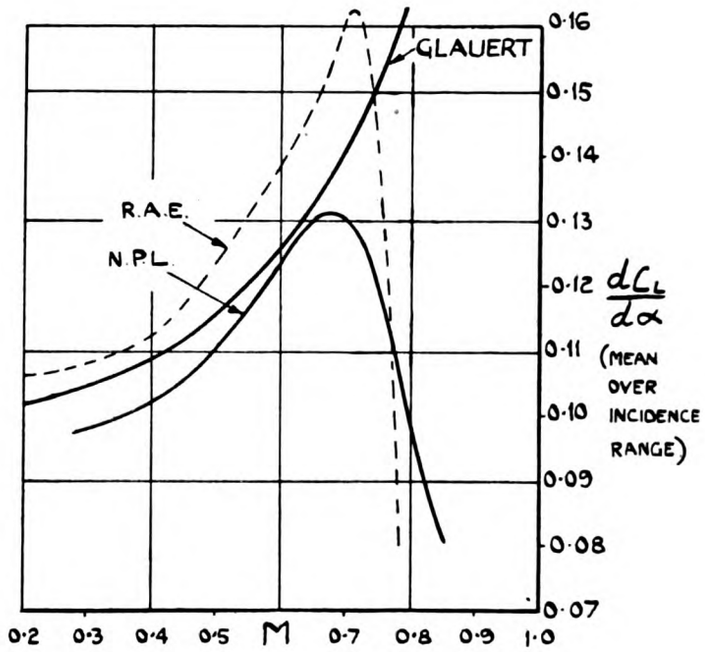

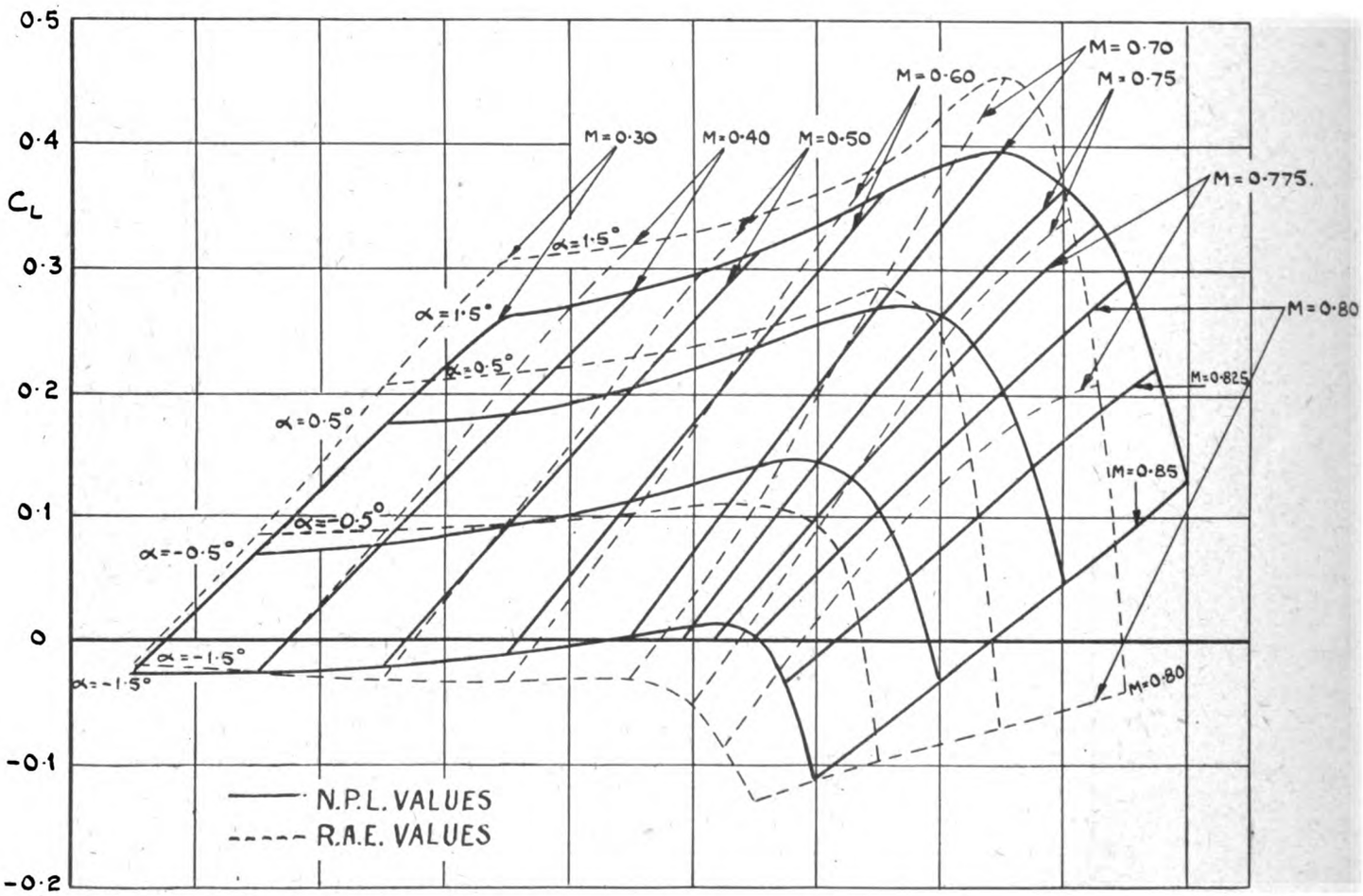

Lift Carpet.

FIG. 9. R.A.E. and N.P.L. High Speed Tunnels.

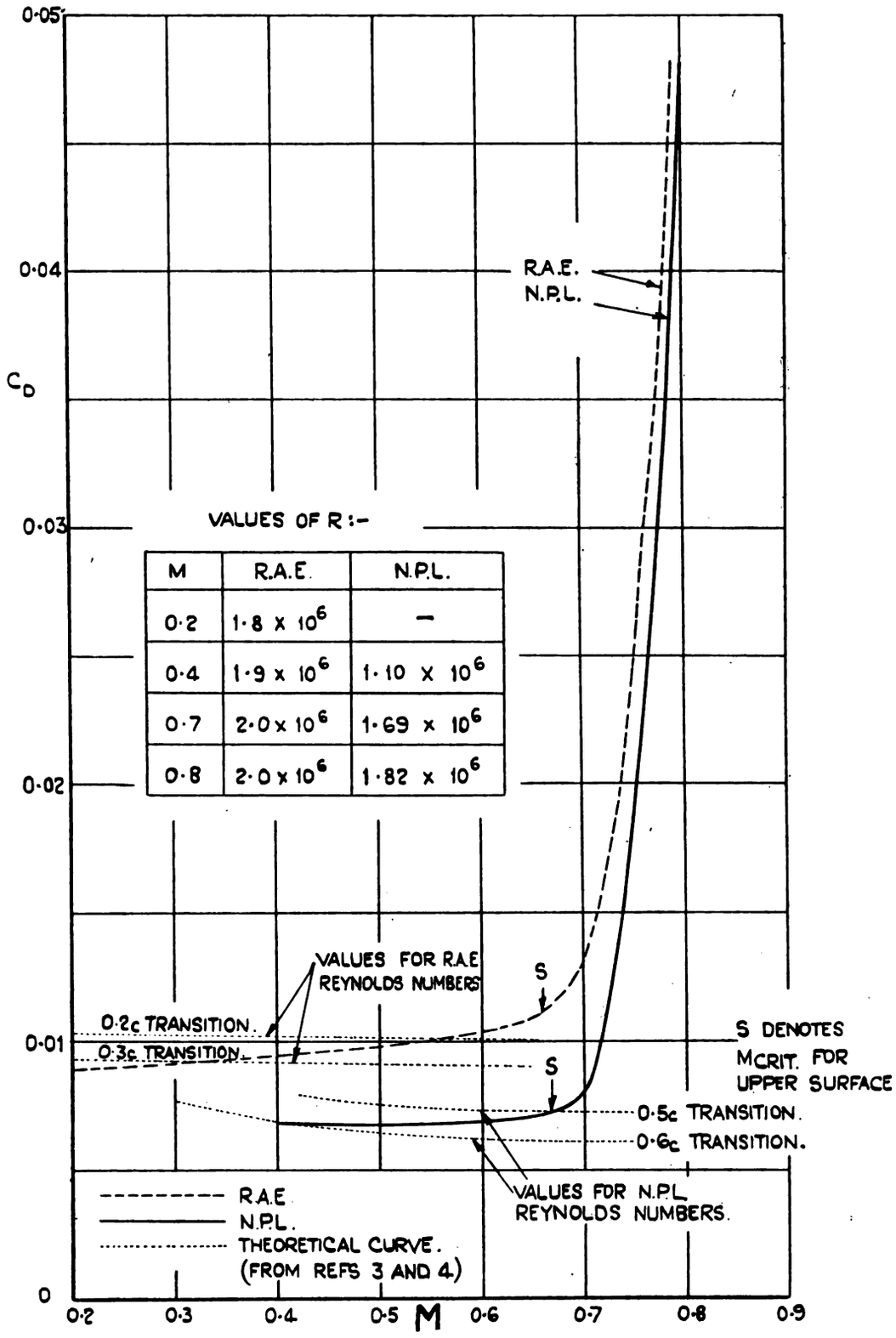

FIG. 10. Wake Traverse Drag. $\alpha = 0$. R.A.E. and N.P.L. High Speed Tunnels.

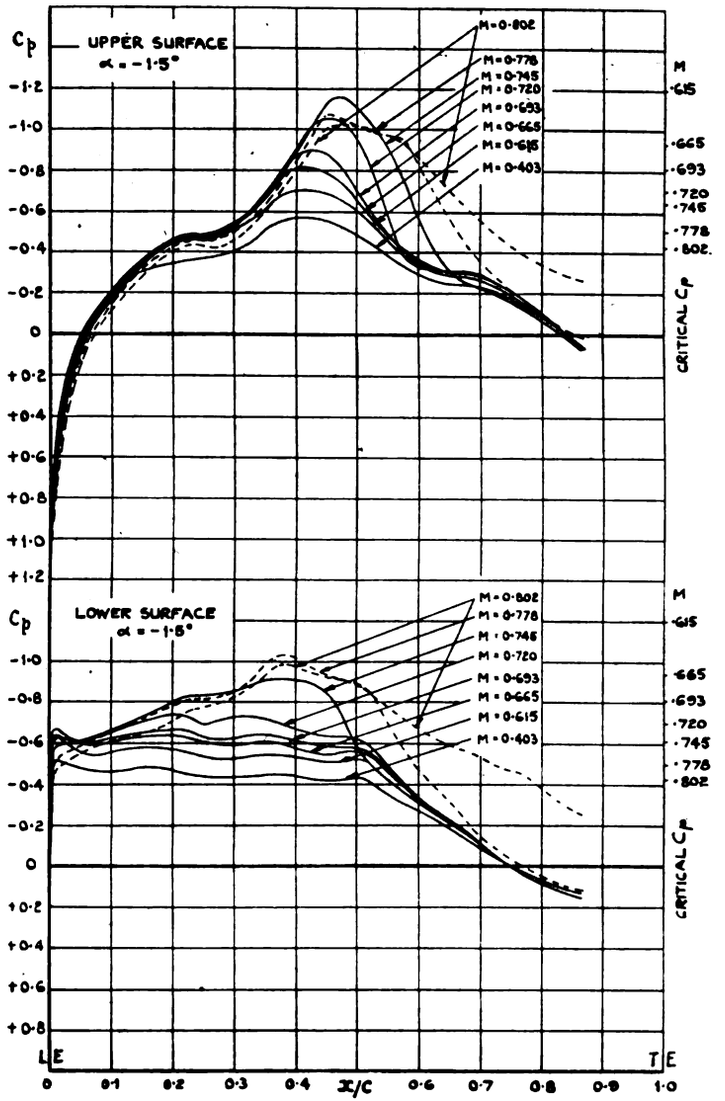

FIG. 11. Pressure Distribution. $\alpha = -1 \cdot 5$ deg.
R.A.E. High Speed Tunnel.

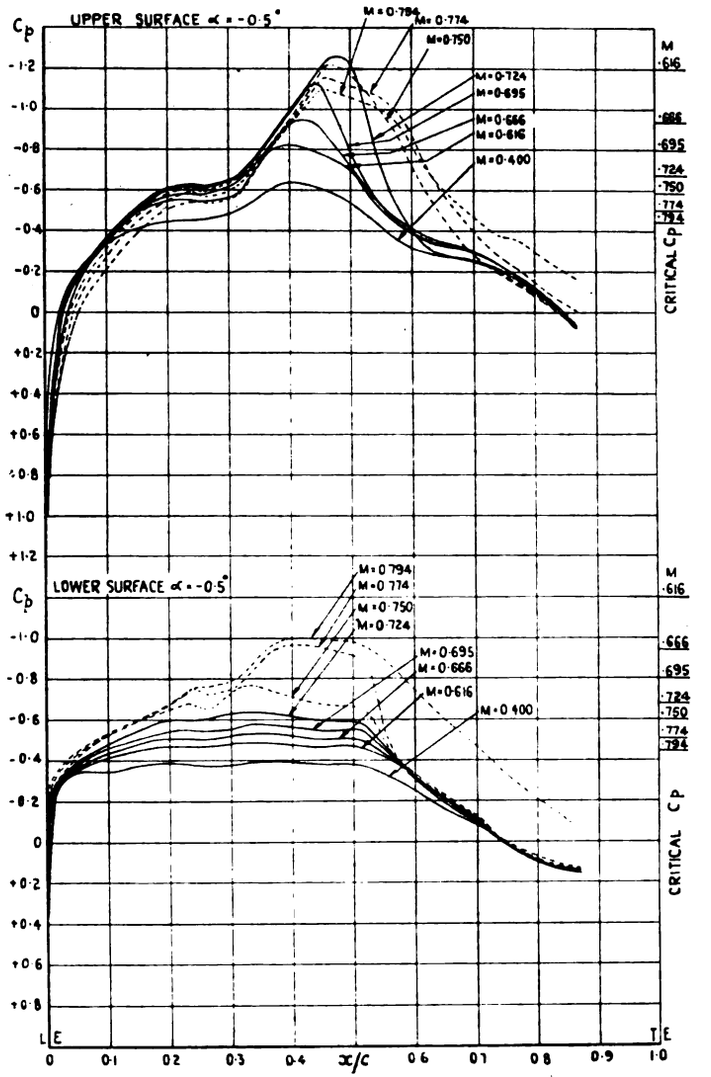

FIG. 12. Pressure Distribution. $\alpha = -0 \cdot 5$ deg.
R.A.E. High Speed Tunnel.

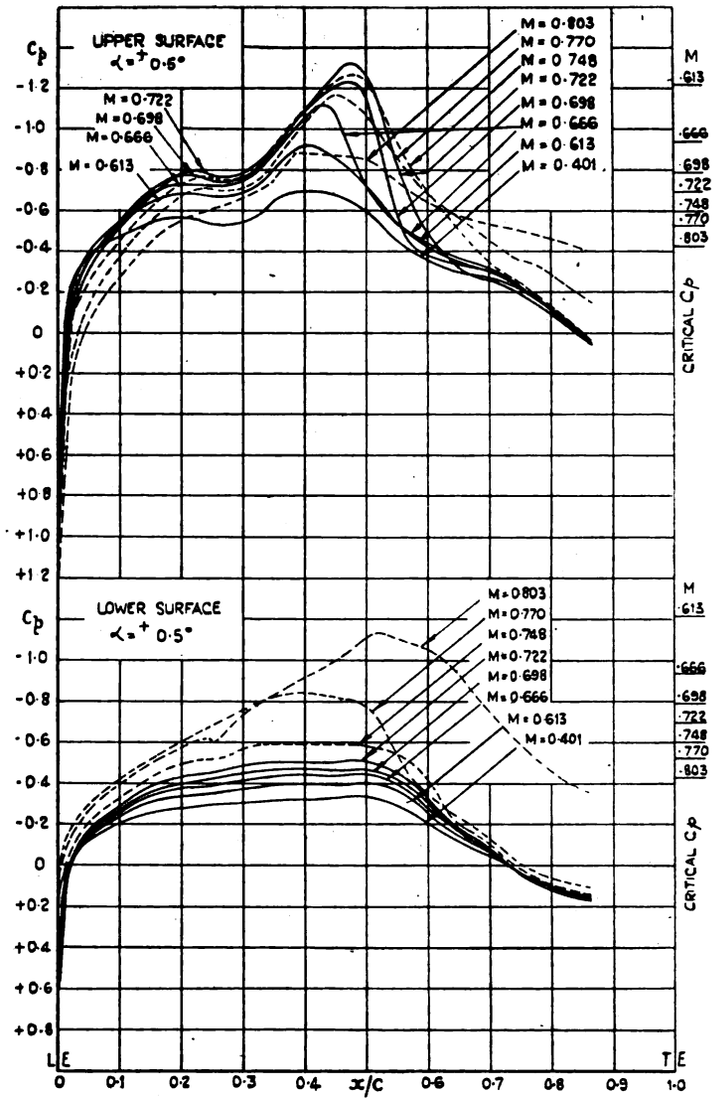

FIG. 13. Pressure Distribution. $\alpha = +0 \cdot 5$ deg.
R.A.E. High Speed Tunnel.

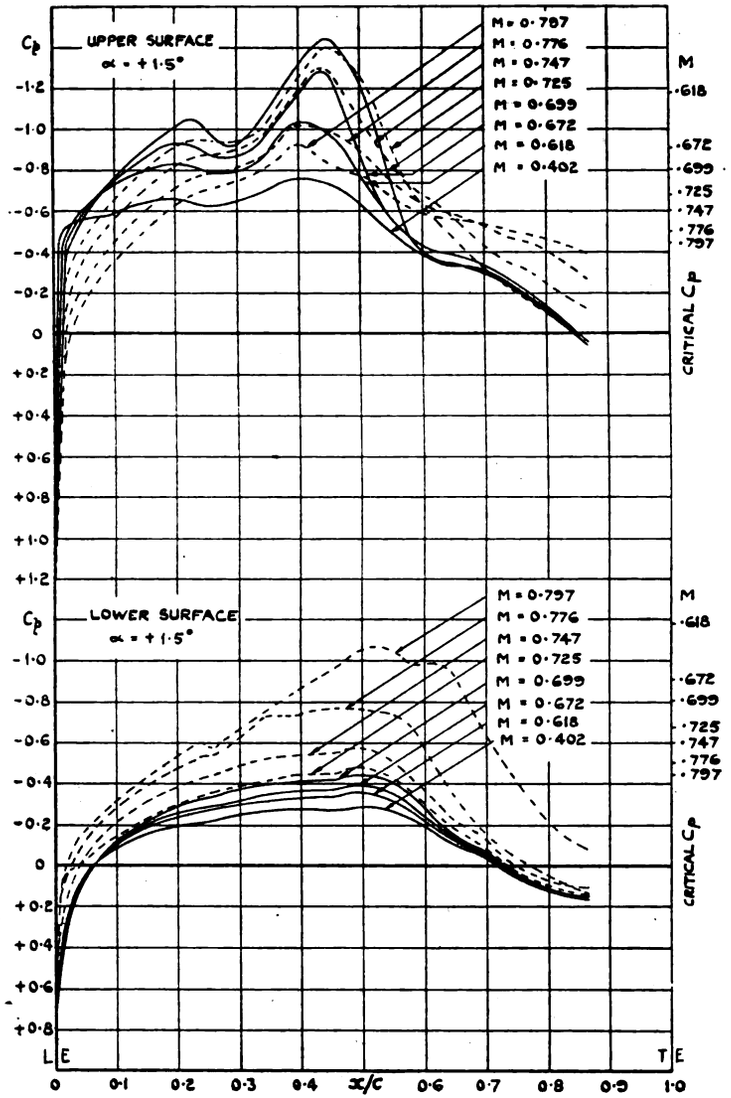

FIG. 14. Pressure Distribution. $\alpha = +1 \cdot 5$ deg.
R.A.E. High Speed Tunnel.

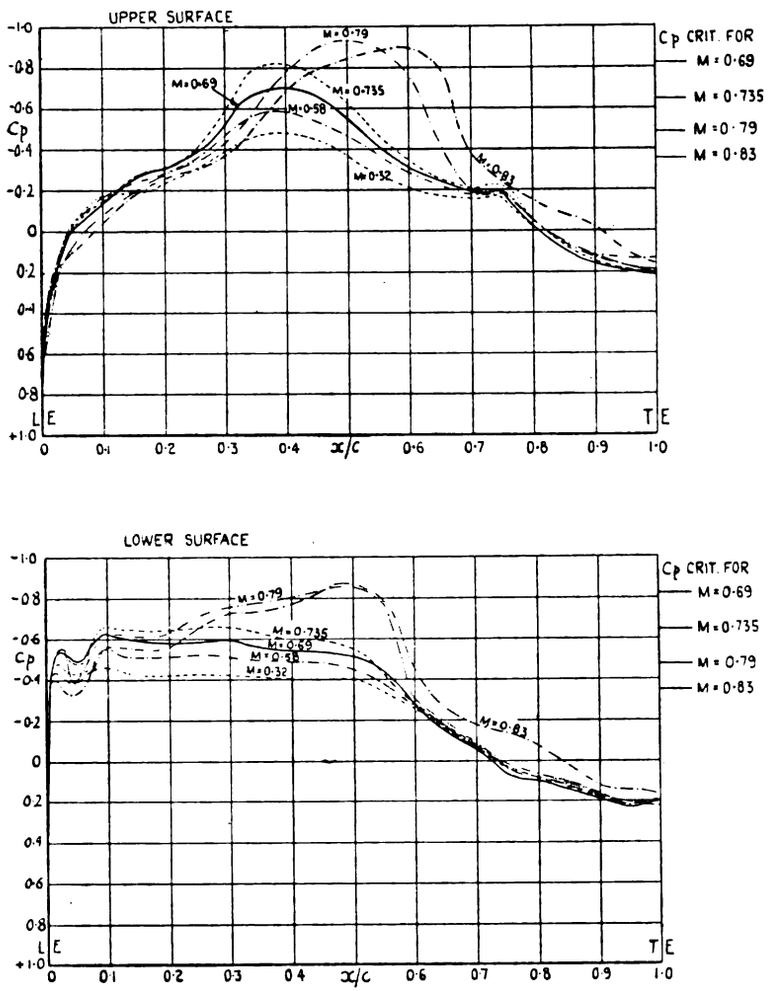

FIG. 15. Pressure Distribution. $\alpha = -2$ deg.
N.P.L. High Speed Tunnel.

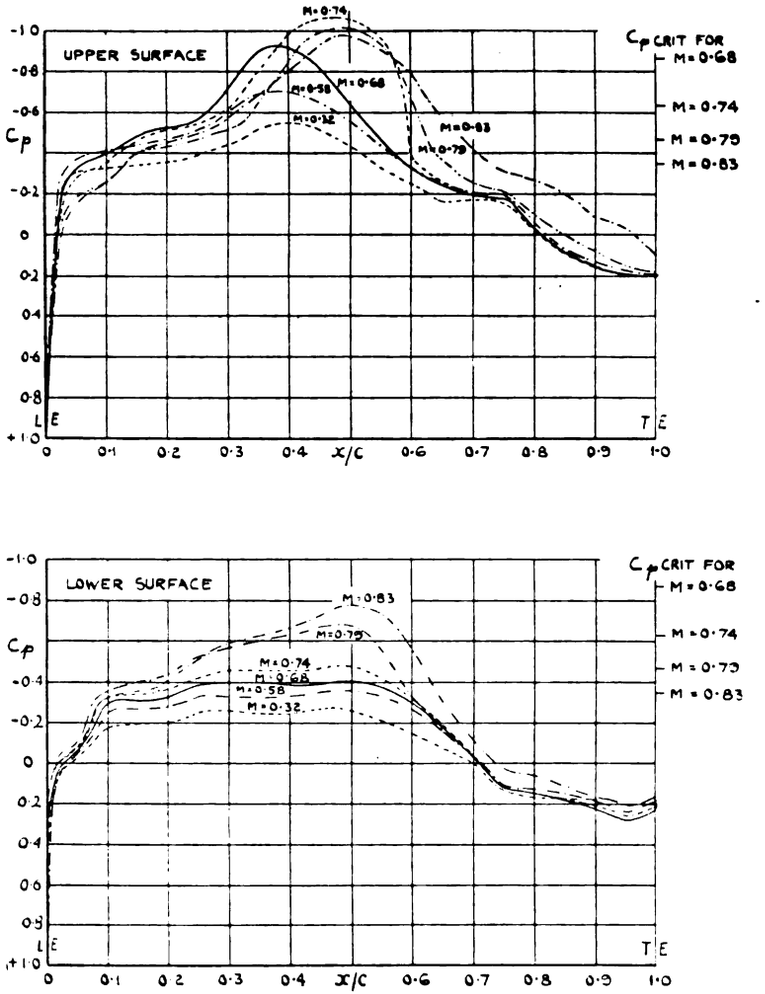

FIG. 16. Pressure Distribution. $\alpha = 0$ deg.
N.P.L. High Speed Tunnel.

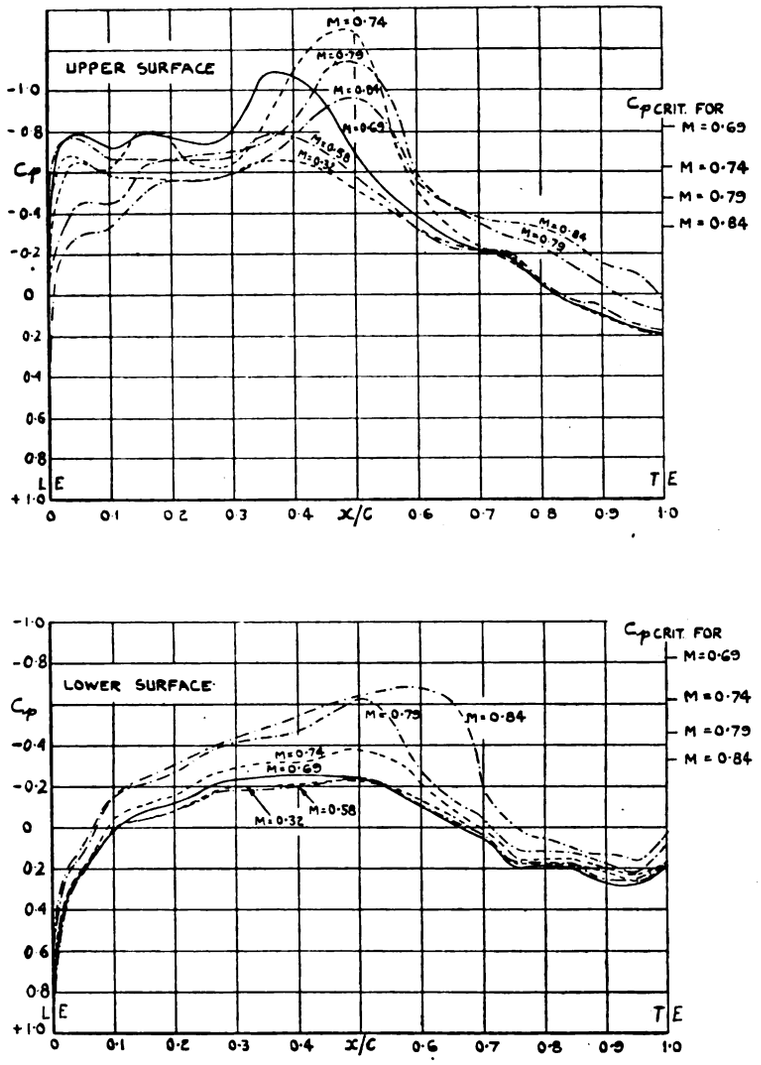

FIG. 17. Pressure Distribution. $\alpha = +2$ deg.
N.P.L. High Speed Tunnel.

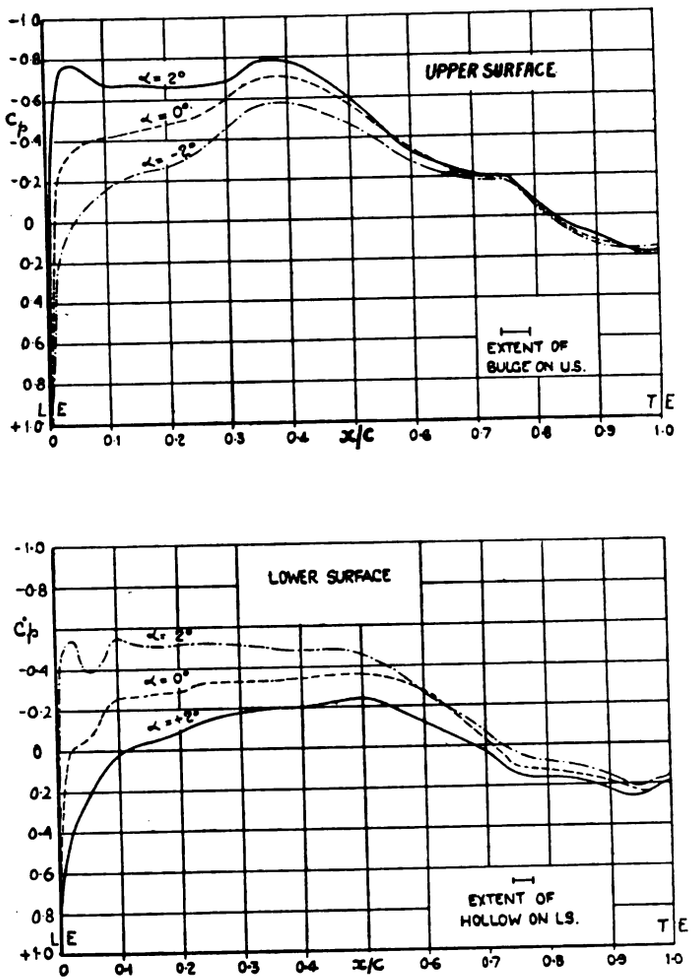

FIG. 18. Pressure Distribution. $M = 0 \cdot 58$.
N.P.L. High Speed Tunnel.

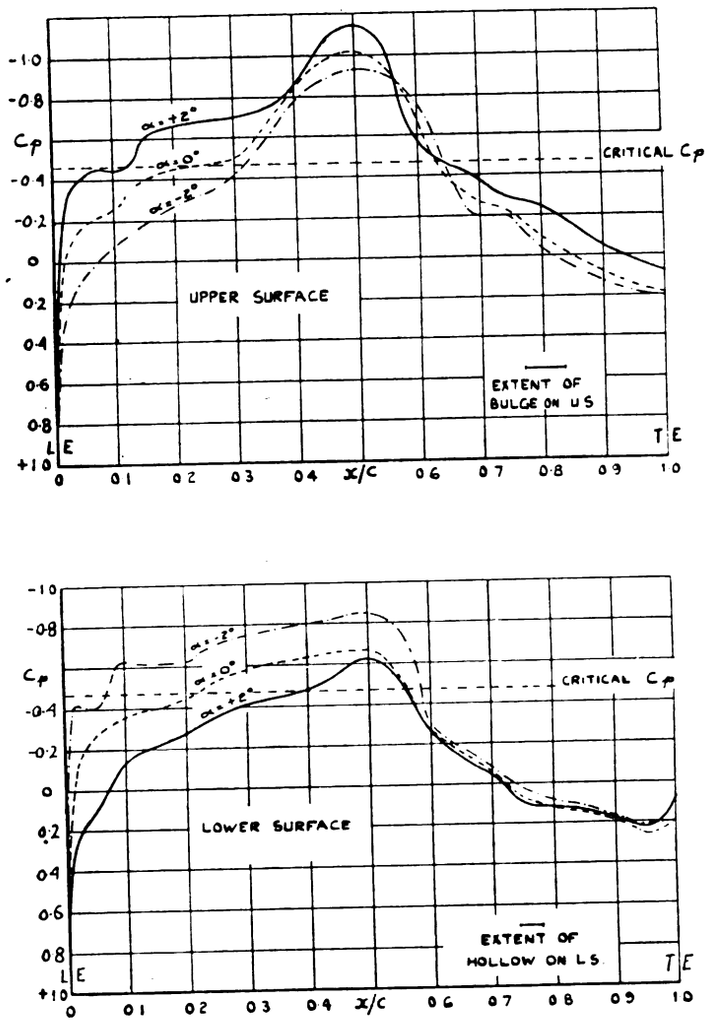

FIG. 19. Pressure Distribution. $M = 0 \cdot 79$.
N.P.L. High Speed Tunnel.

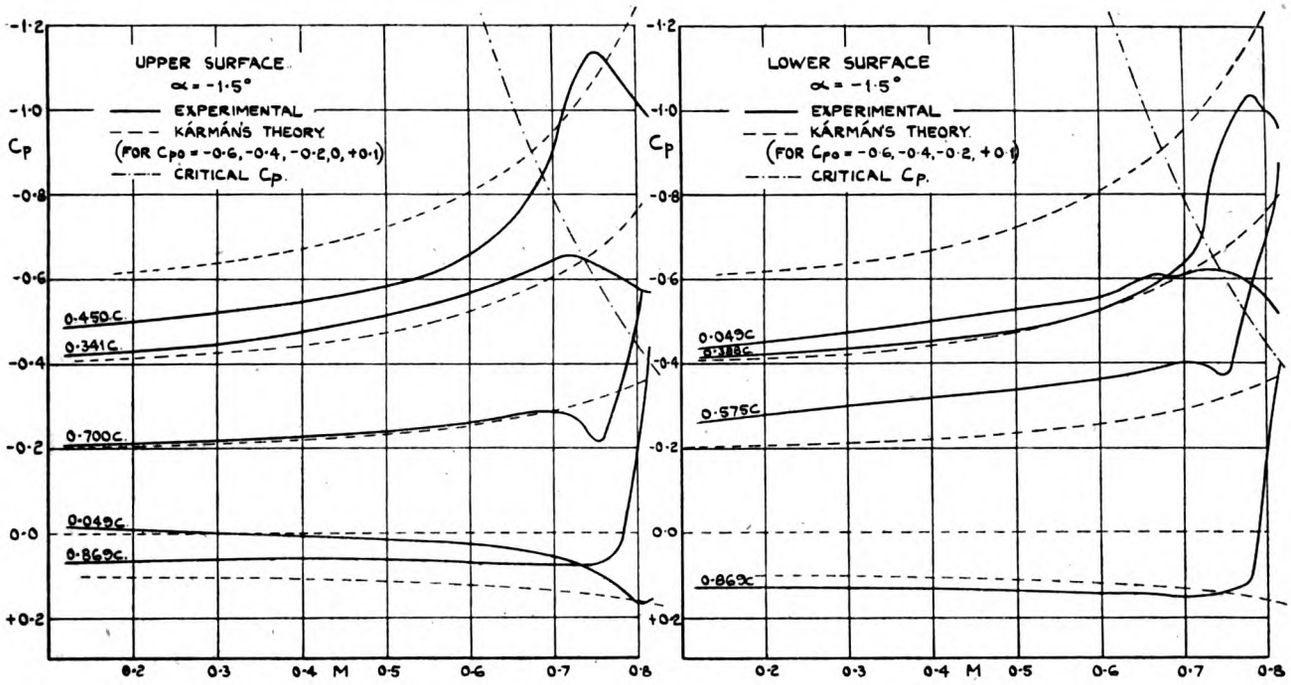

FIG. 20. Variation of C_p with M. $\alpha = -1 \cdot 5$ deg. R.A.E. High Speed Tunnel.

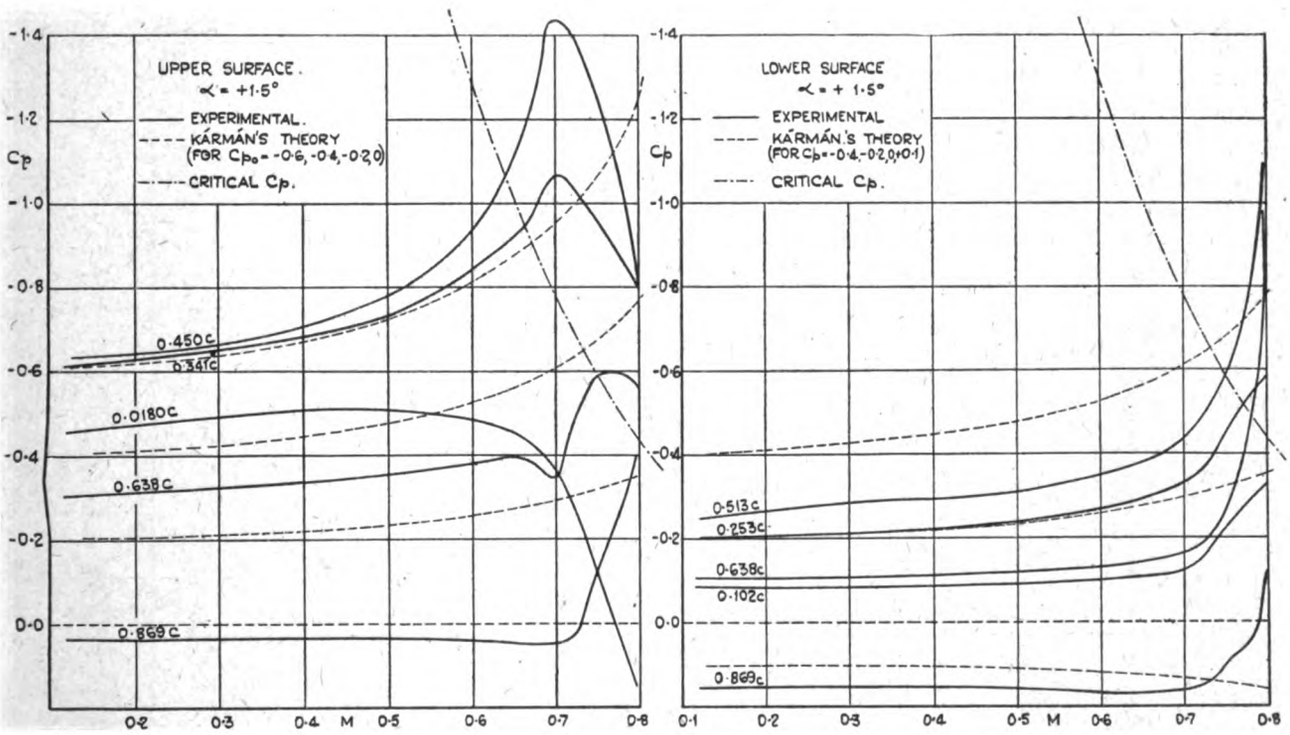

FIG. 21. Variation of C_p with M. $\alpha = +1 \cdot 5$ deg. R.A.E. High Speed Tunnel.

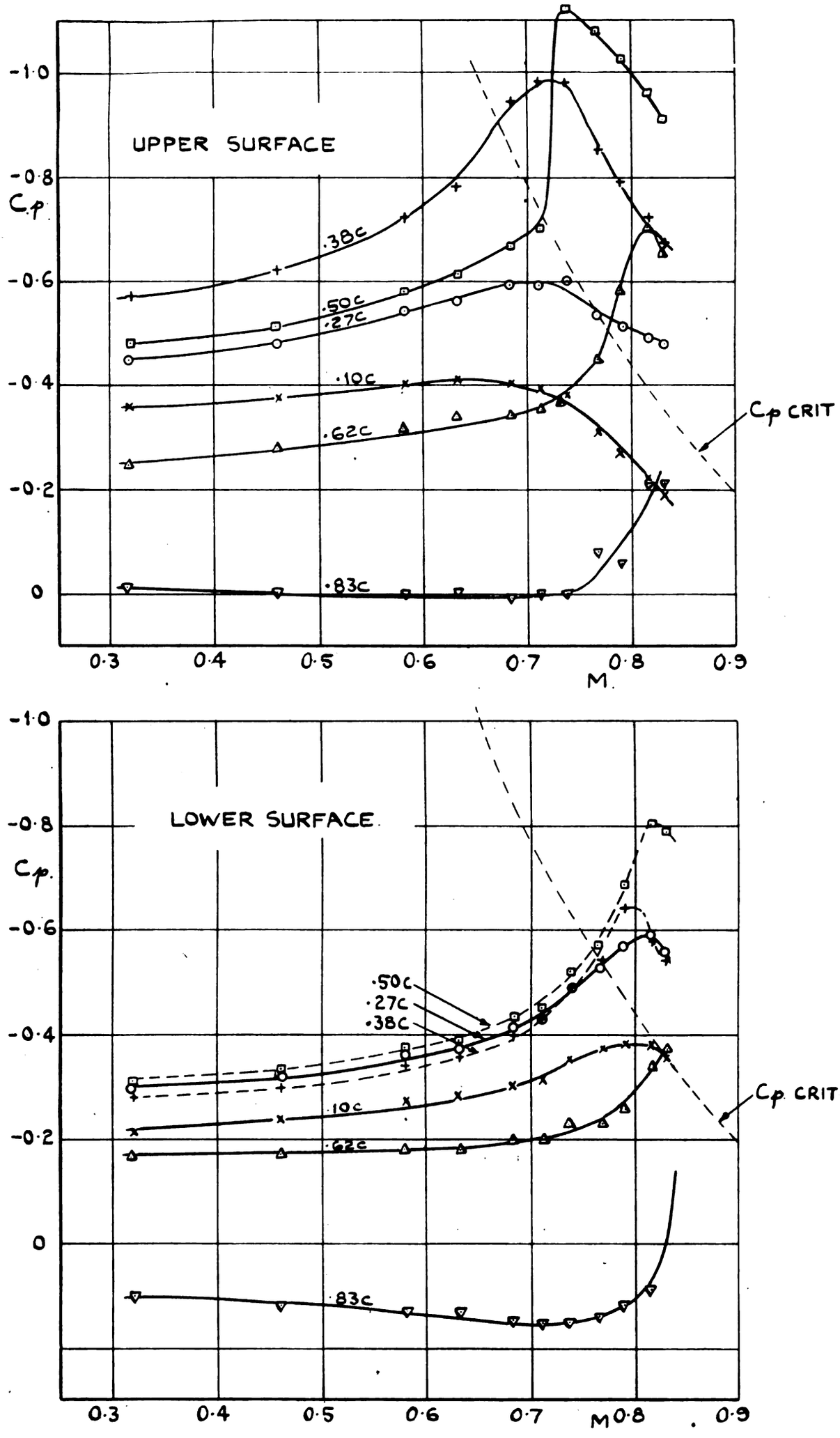

FIG. 22. Variation of C_p with M at Various Holes on the Surface for $\alpha = 0$ deg. N.P.L. Tests.

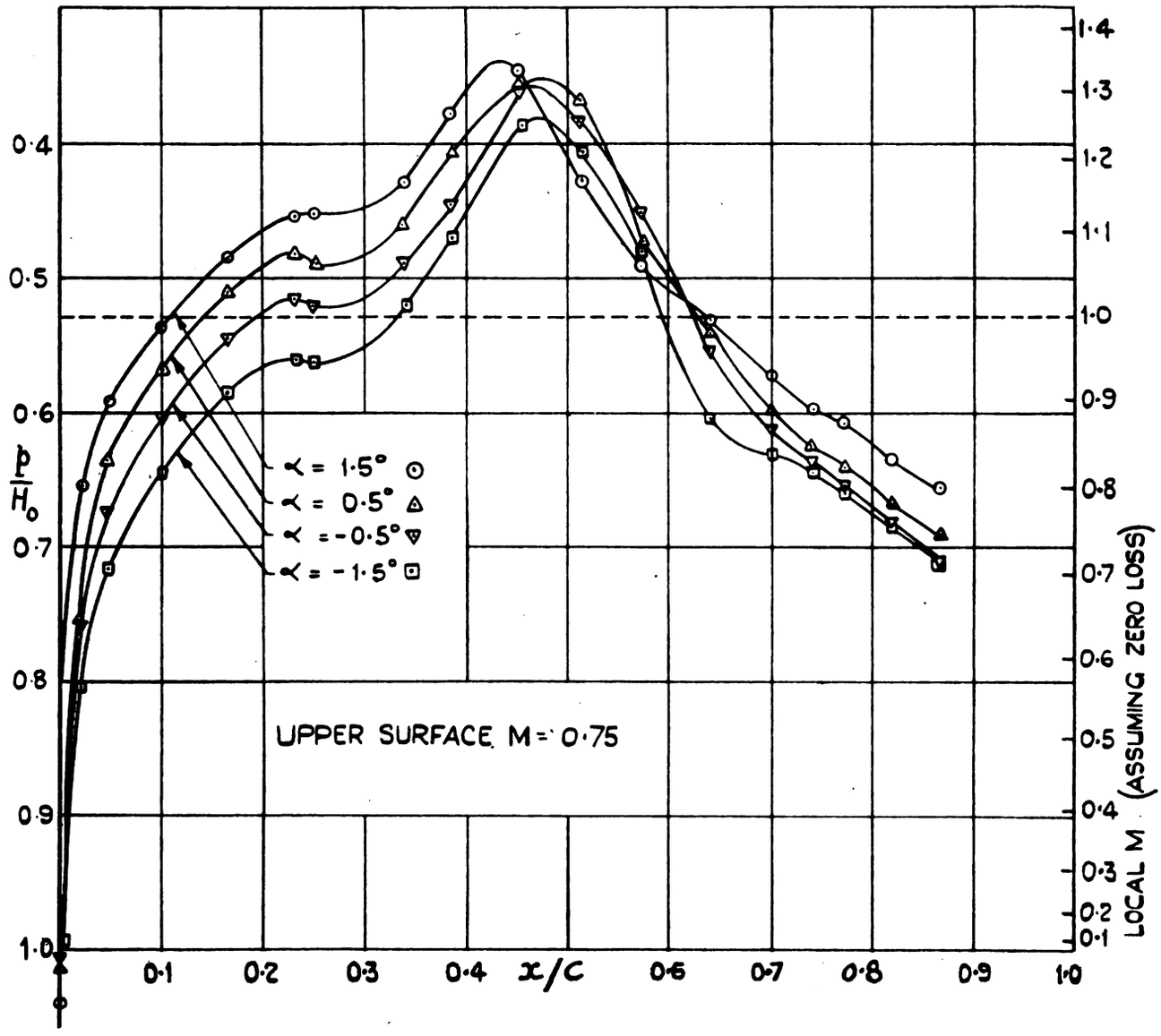
UPPER SURFACE M = 0·75
α = 1·5° ⊙
α = 0·5° △
α = -0·5° ▽
α = -1·5° ⊡
p/H₀
x/C
LOCAL M (ASSUMING ZERO LOSS)

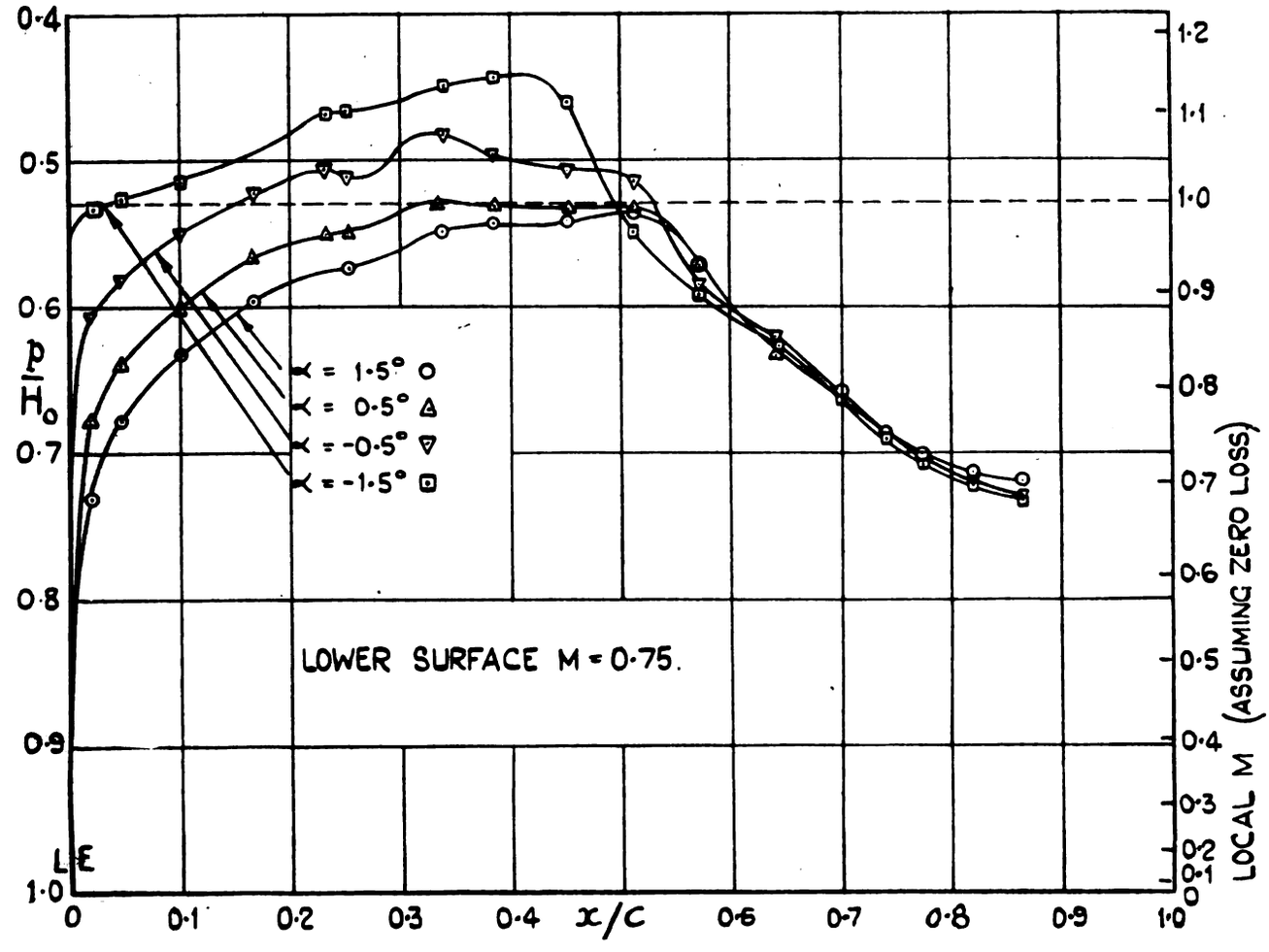
LOWER SURFACE M = 0·75.
α = 1·5° O
α = 0·5° △
α = -0·5° ▽
α = -1·5° ⊡
L.E
p/H₀
x/C
LOCAL M (ASSUMING ZERO LOSS)

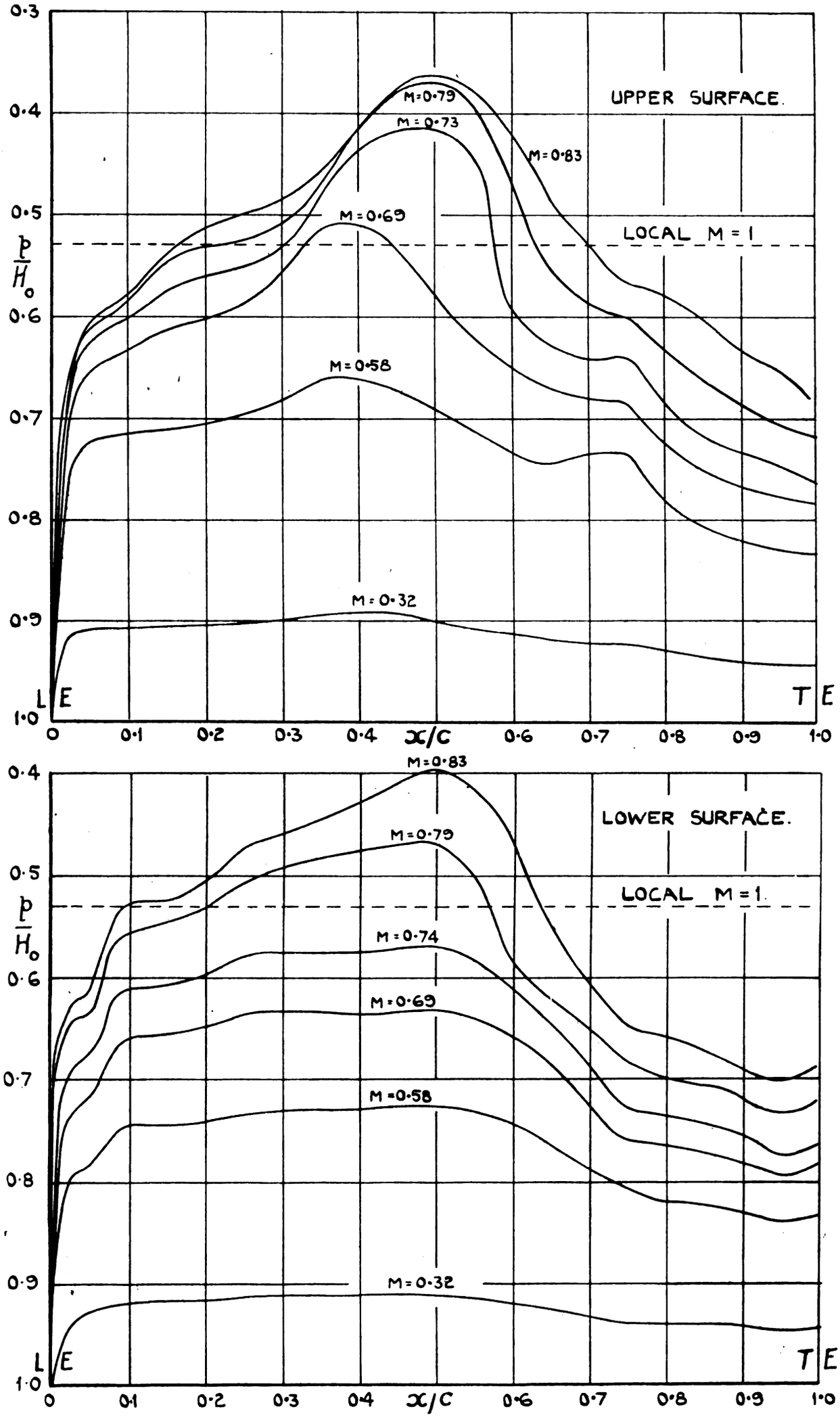

FIG. 24. Pressure Distribution. p/H_0. $\alpha = -1$ deg. N.P.L. High Speed Tunnel.

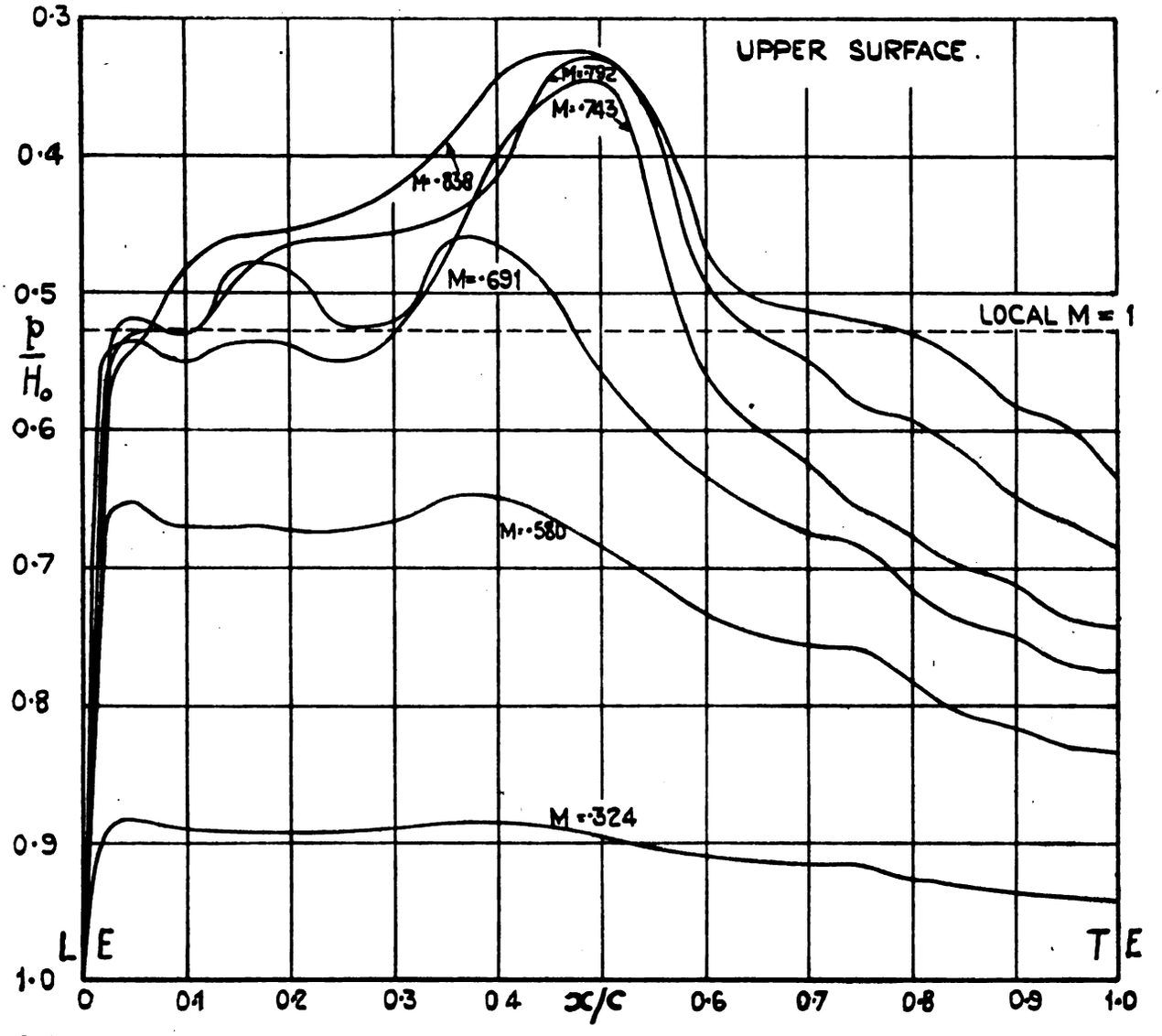
UPPER SURFACE.
M=·792
M=·743
M=·838
M=·691
LOCAL M = 1
M=·580
M=·324
p/H₀
0·3
0·4
0·5
0·6
0·7
0·8
0·9
1·0
L E
T E
0
0·1
0·2
0·3
0·4
x/c
0·6
0·7
0·8
0·9
1·0

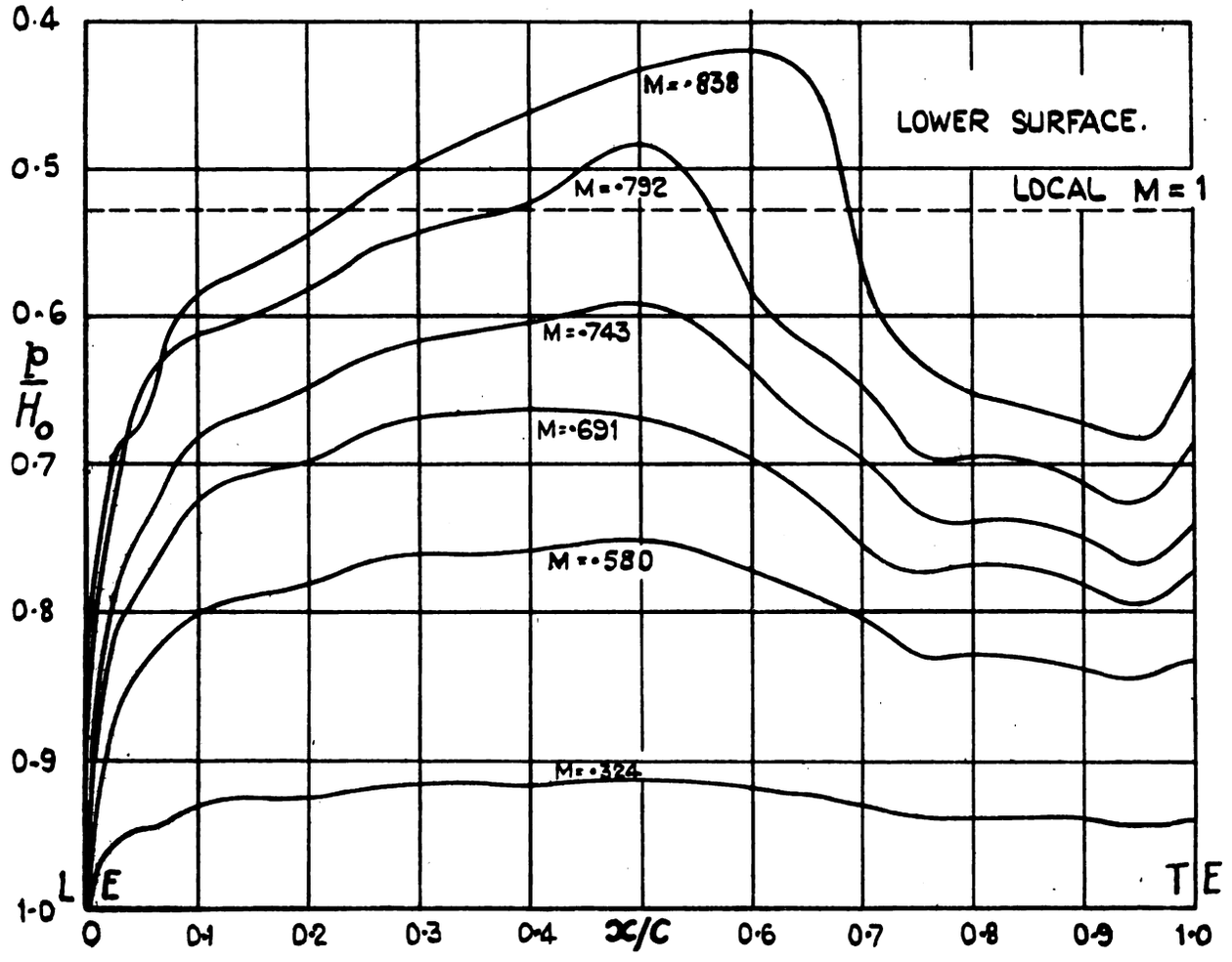
M=·838
LOWER SURFACE.
M=·792
LOCAL M = 1
M=·743
M=·691
M=·580
M=·324
p/H₀
0·4
0·5
0·6
0·7
0·8
0·9
1·0
L E
T E
0
0·1
0·2
0·3
0·4
x/c
0·6
0·7
0·8
0·9
1·0

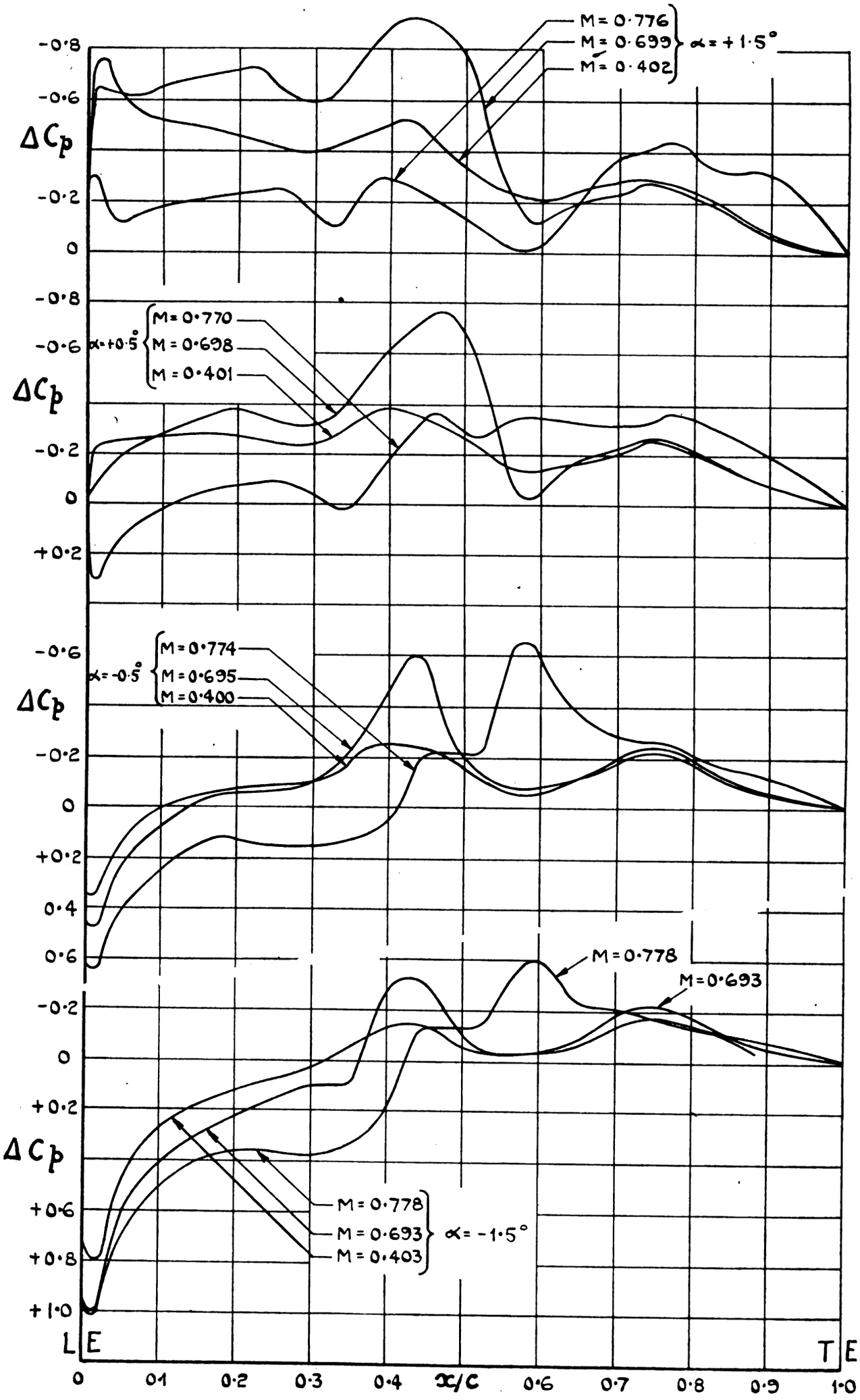

FIG. 26. Lift Distribution. R.A.E. High Speed Tunnel.

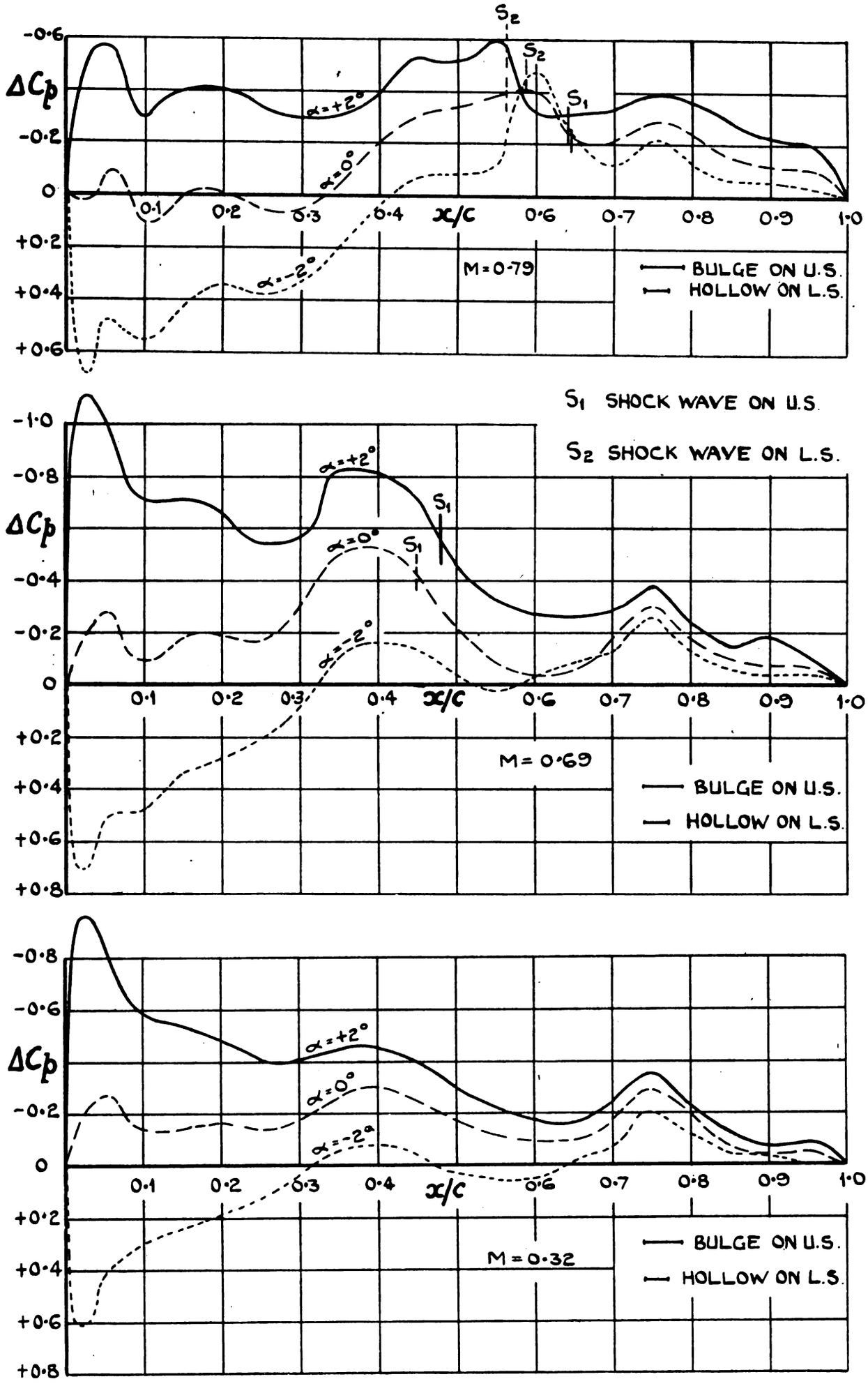

FIG. 27. Lift Distribution. N.P.L. High Speed Tunnel.

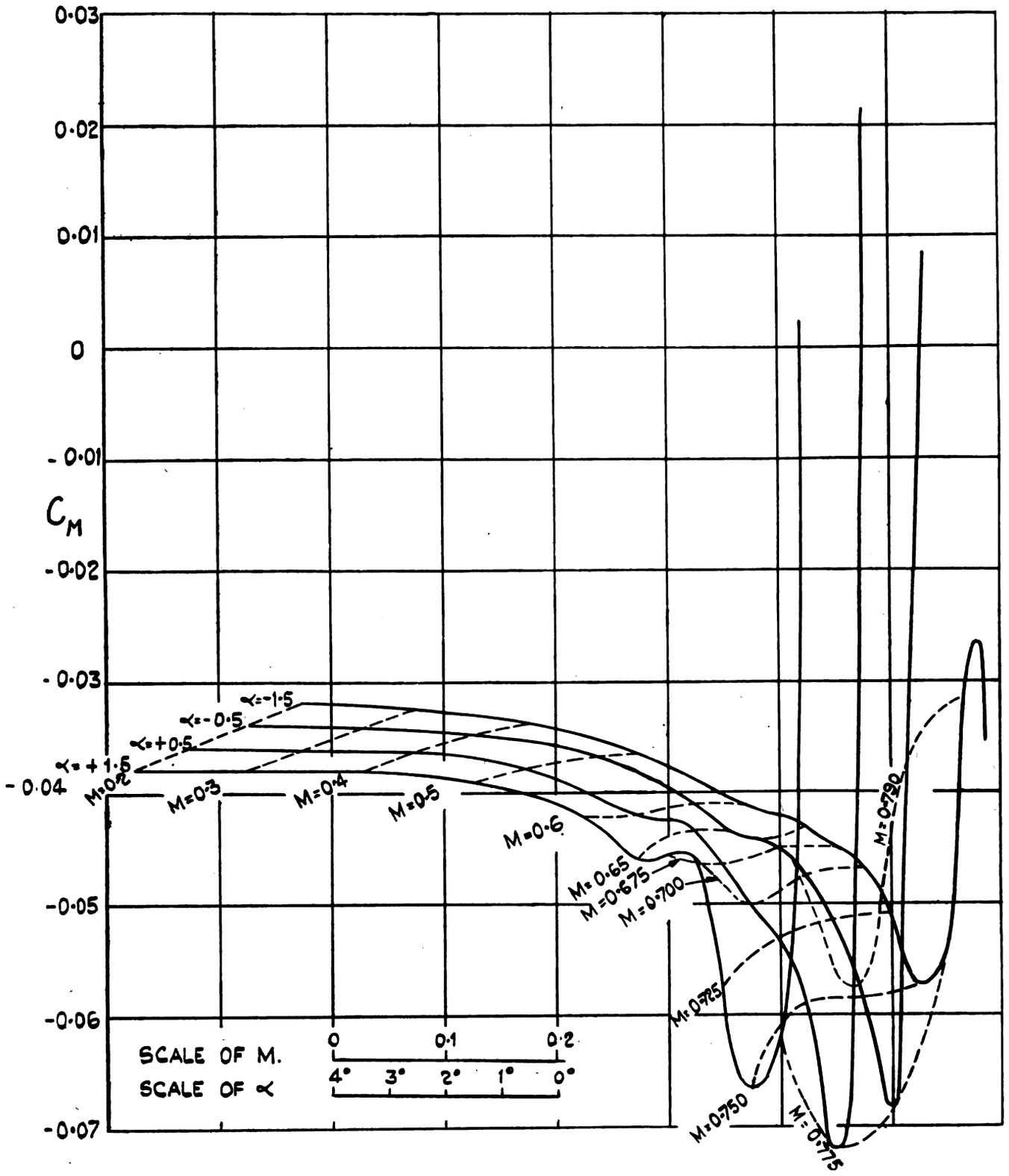

FIG. 28. C_M Carpet. R.A.E. High Speed Tunnel.

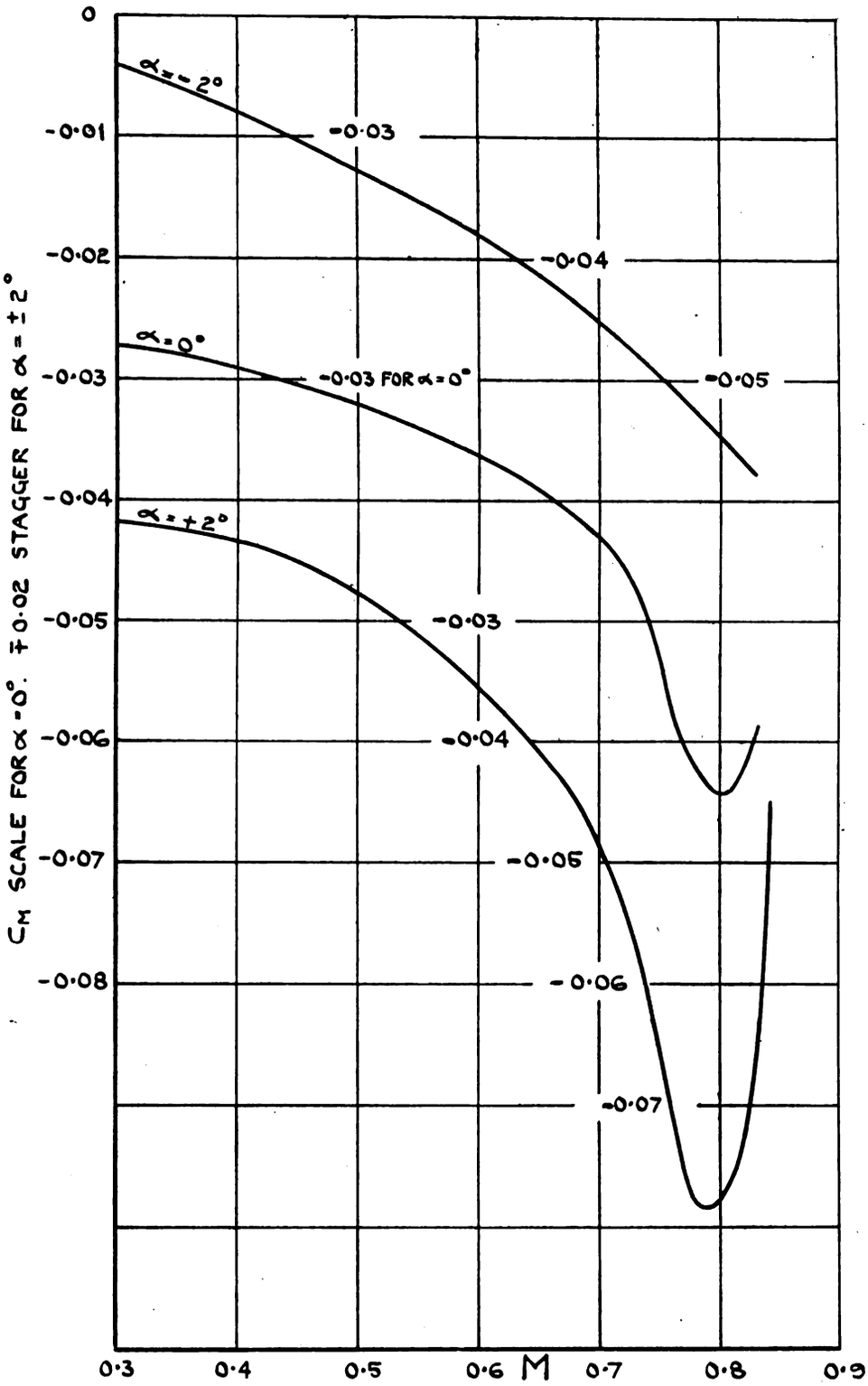

FIG. 29. Variation of C_M with Mach Number. N.P.L. High Speed Tunnel.

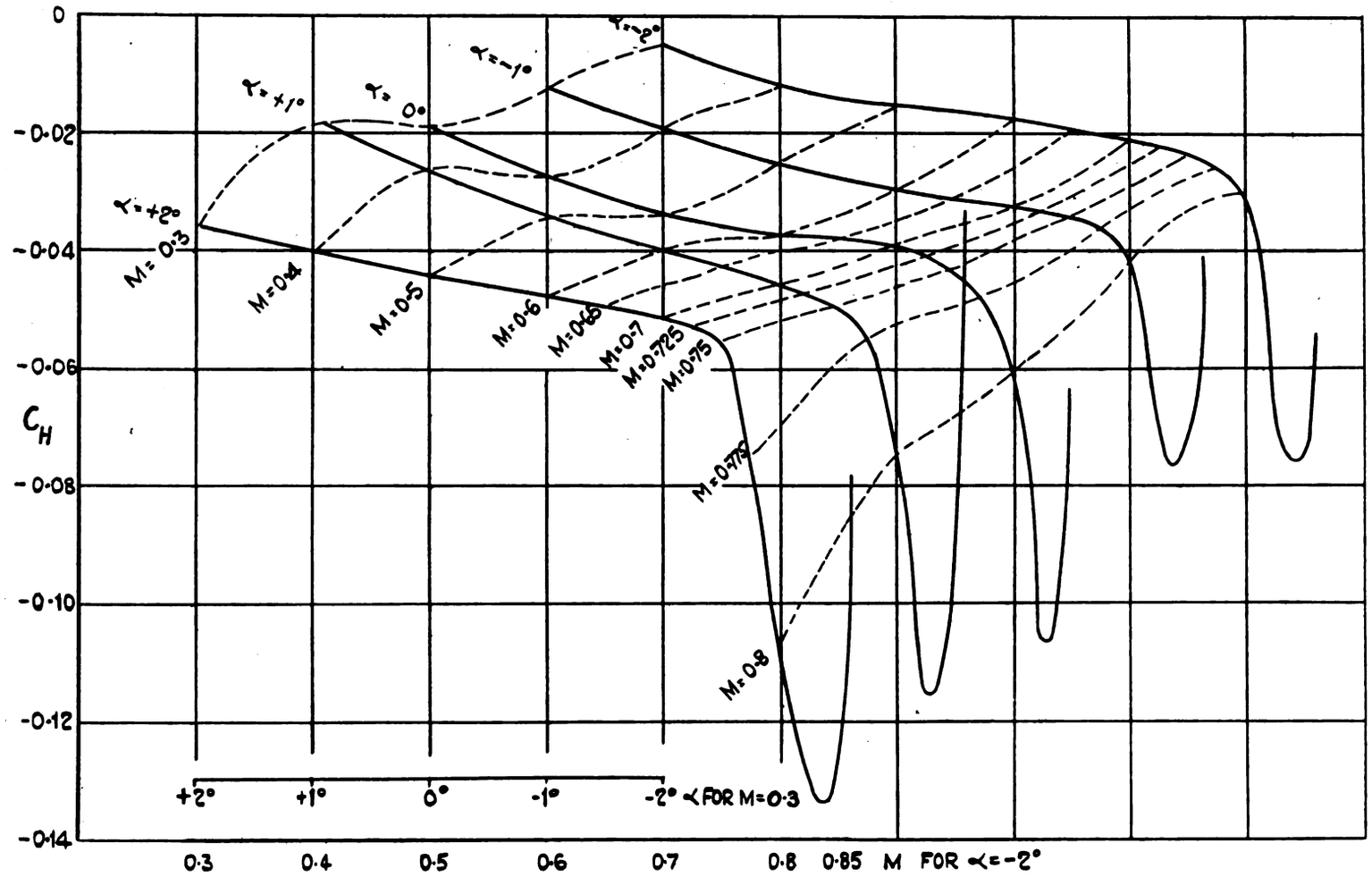

FIG. 30. 0·75*c* Hinge Moment Carpet. N.P.L. Tests.

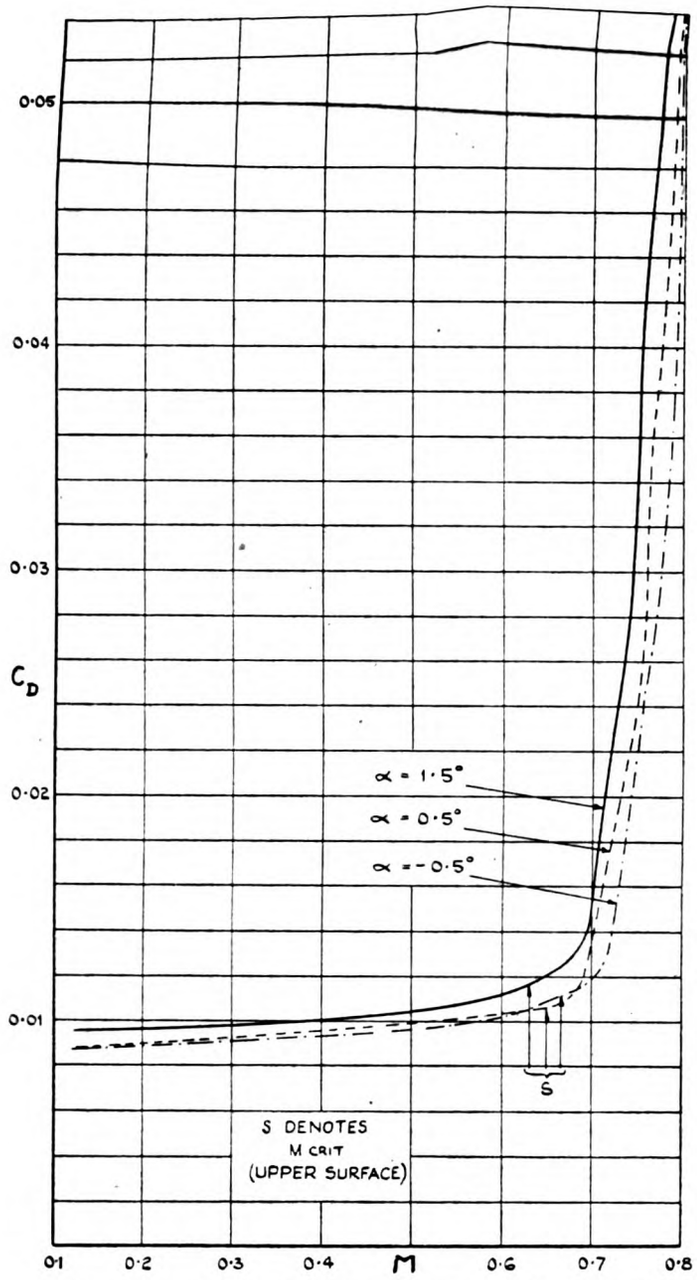

FIG. 31. Drag from Wake Traverse. ($R = 2 \times 10^6$) R.A.E. High Speed Tunnel.

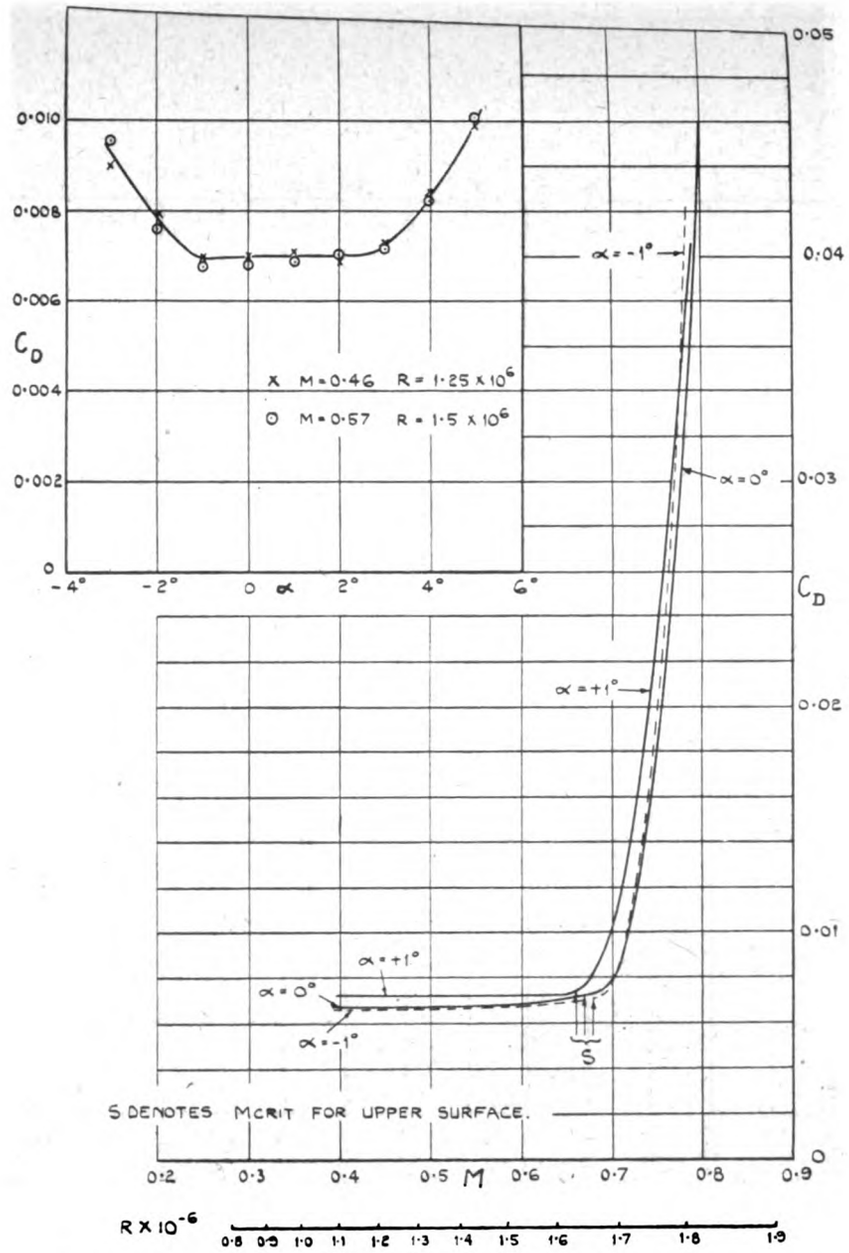

FIG. 32. Drag from Wake Traverse. N.P.L. High Speed Tunnel.

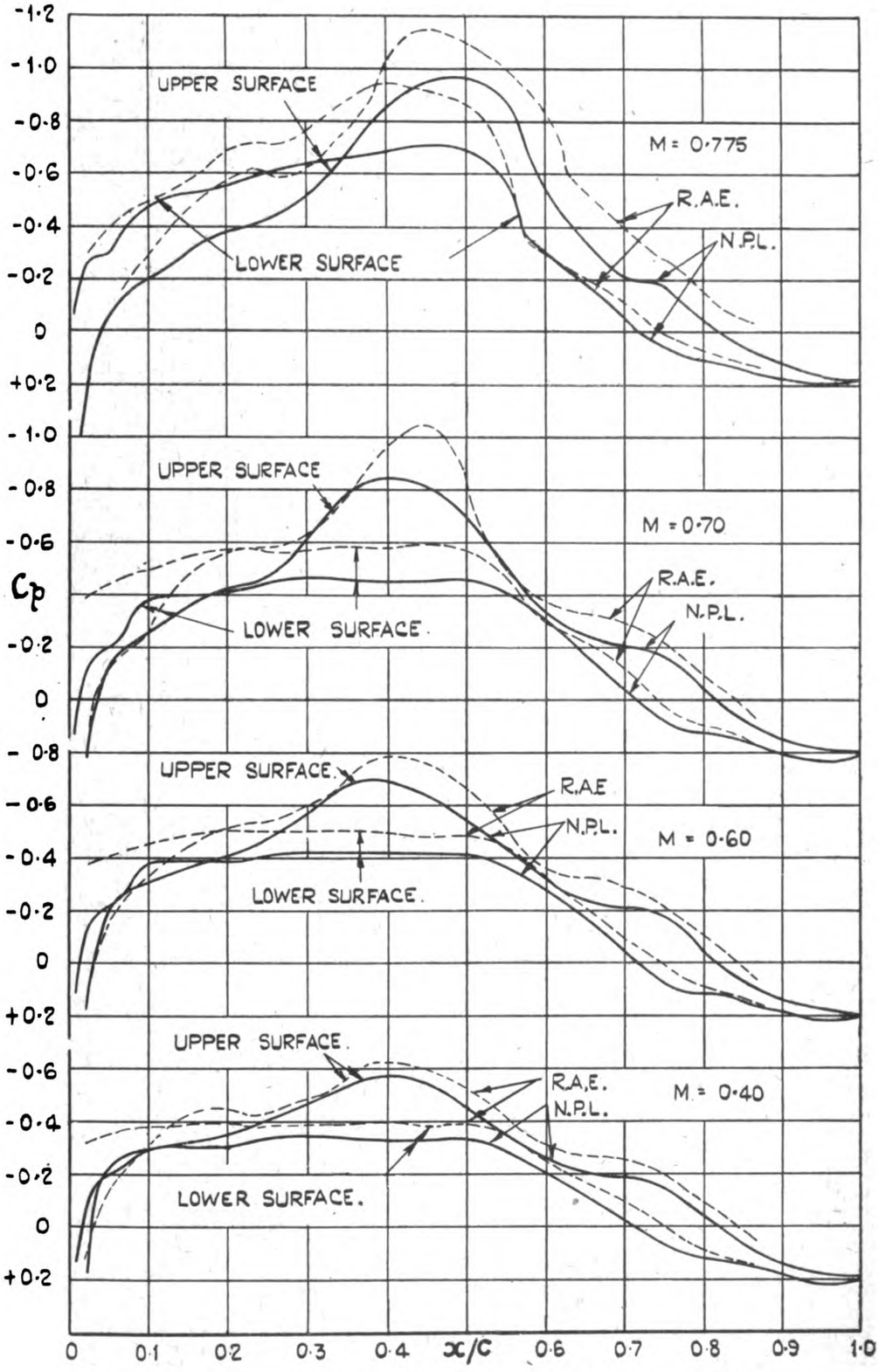

FIG. 33. Pressure Distribution. $C_L = 0 \cdot 07$. R.A.E. and N.P.L. Tests.

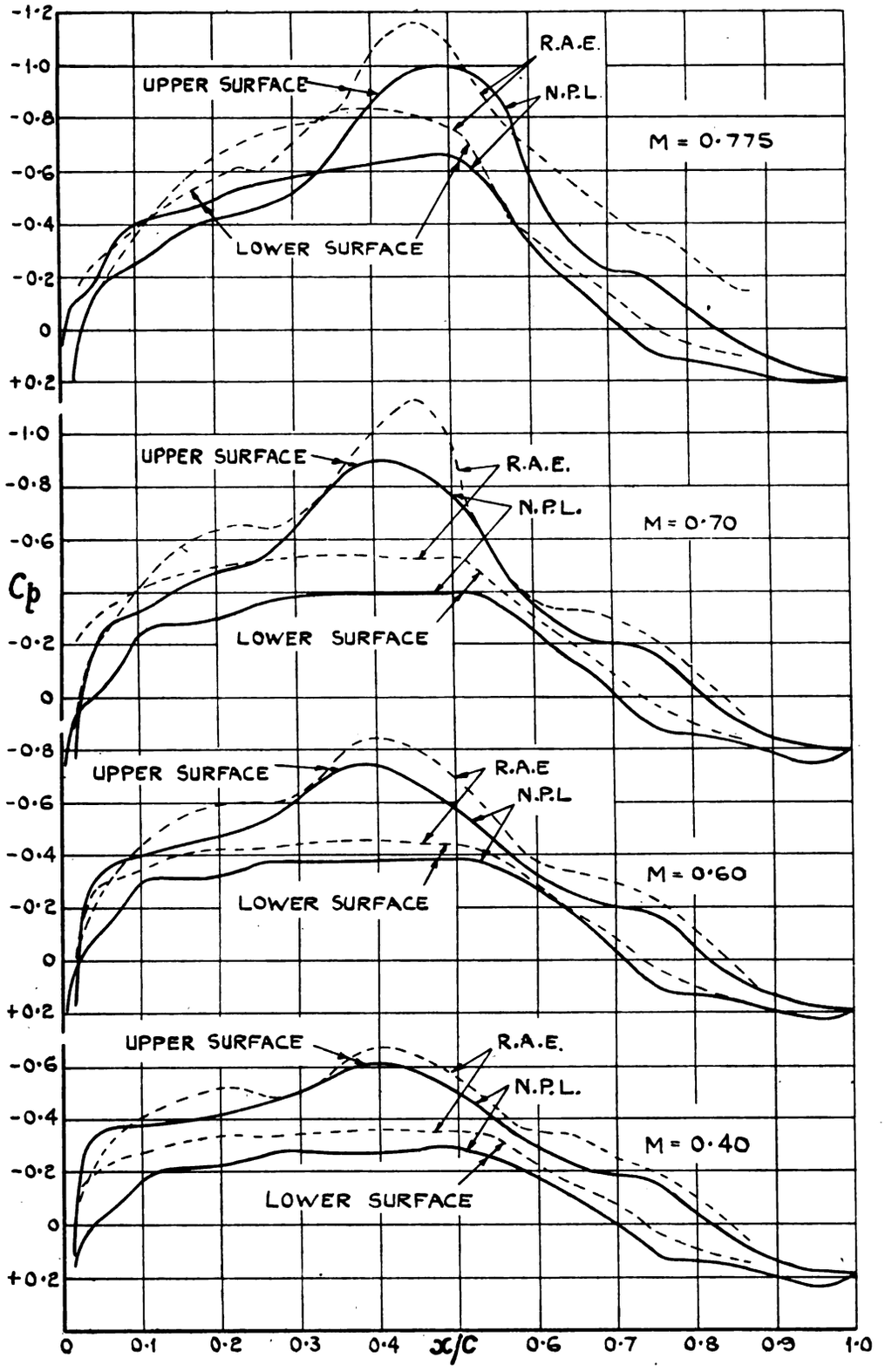

FIG. 34. Pressure Distribution. $C_L = 0 \cdot 15$. R.A.E. and N.P.L. Tests.

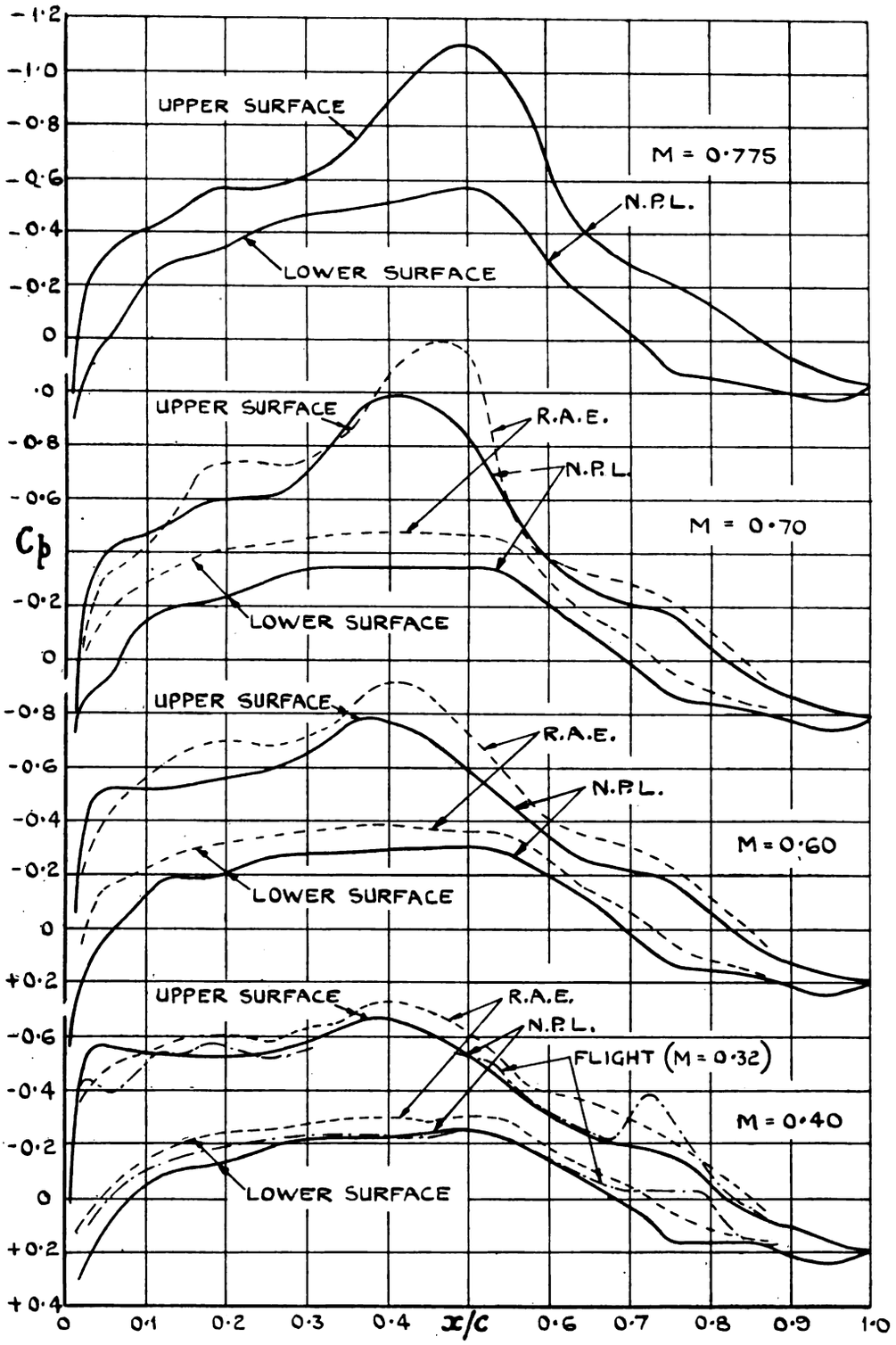

FIG. 35. Pressure Distribution. $C_L = 0 \cdot 27$. R.A.E. and N.P.L. Tests.

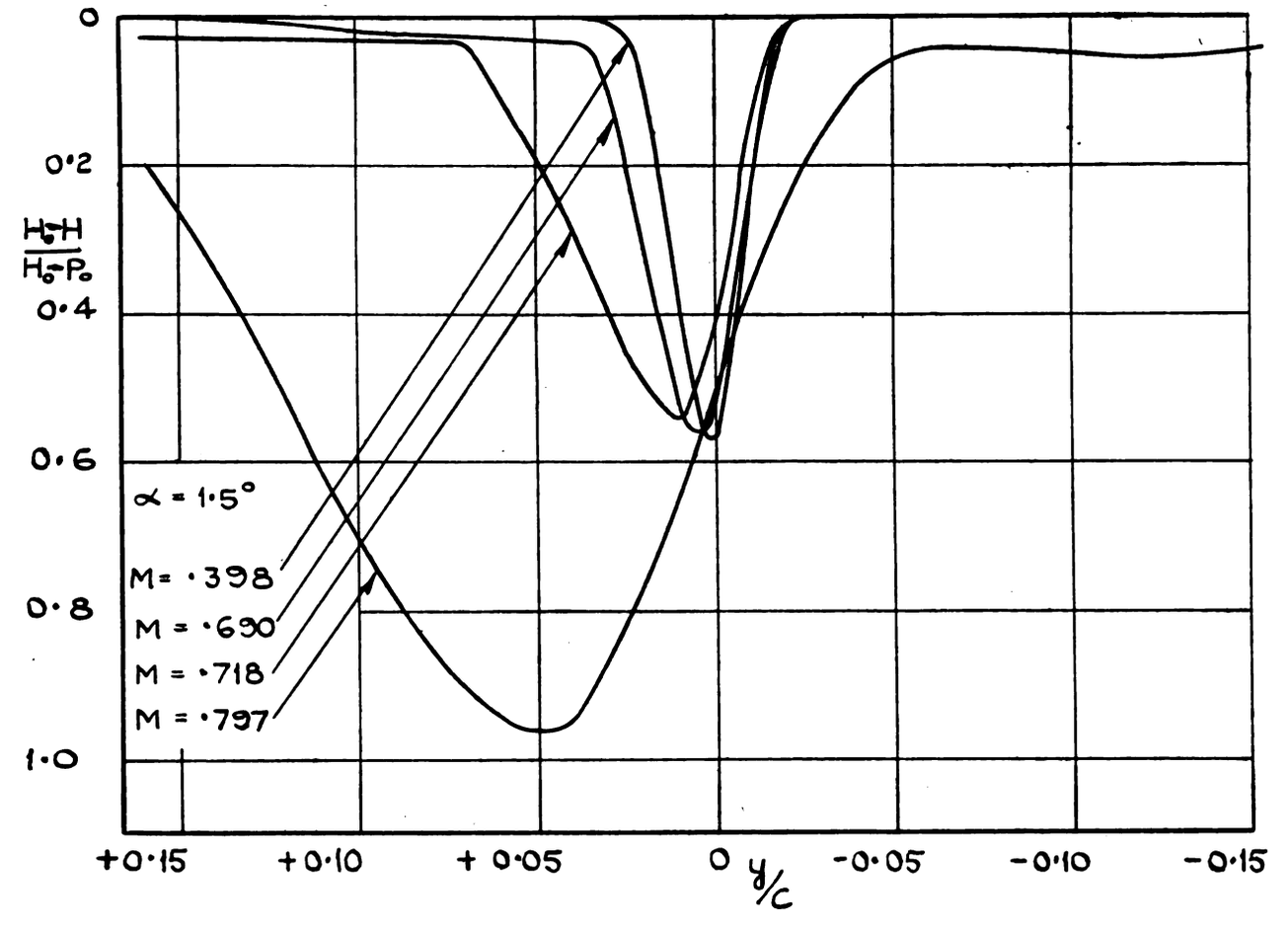

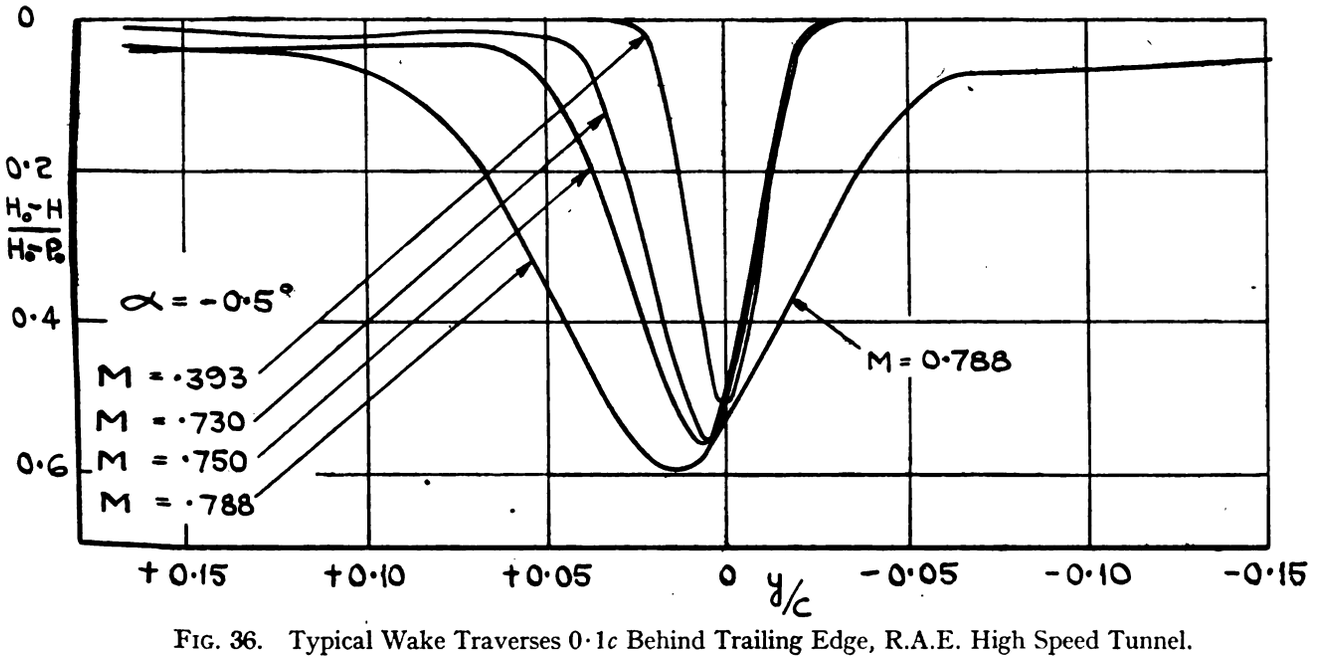

FIG. 36. Typical Wake Traverses 0·1*c* Behind Trailing Edge, R.A.E. High Speed Tunnel.

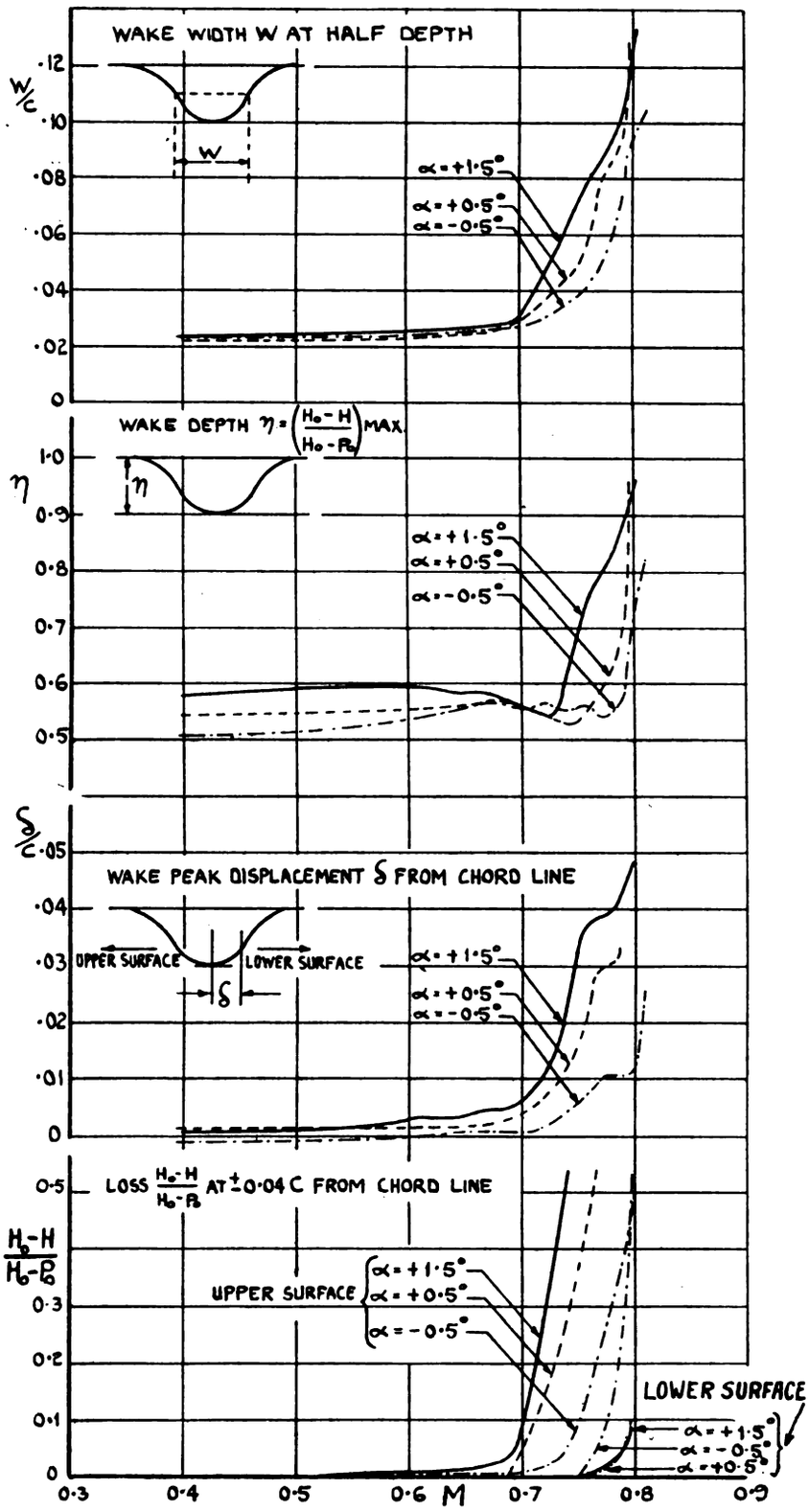

FIG. 37. Wake at 0·1*c* Behind Trailing Edge, R.A.E. High Speed Tunnel.

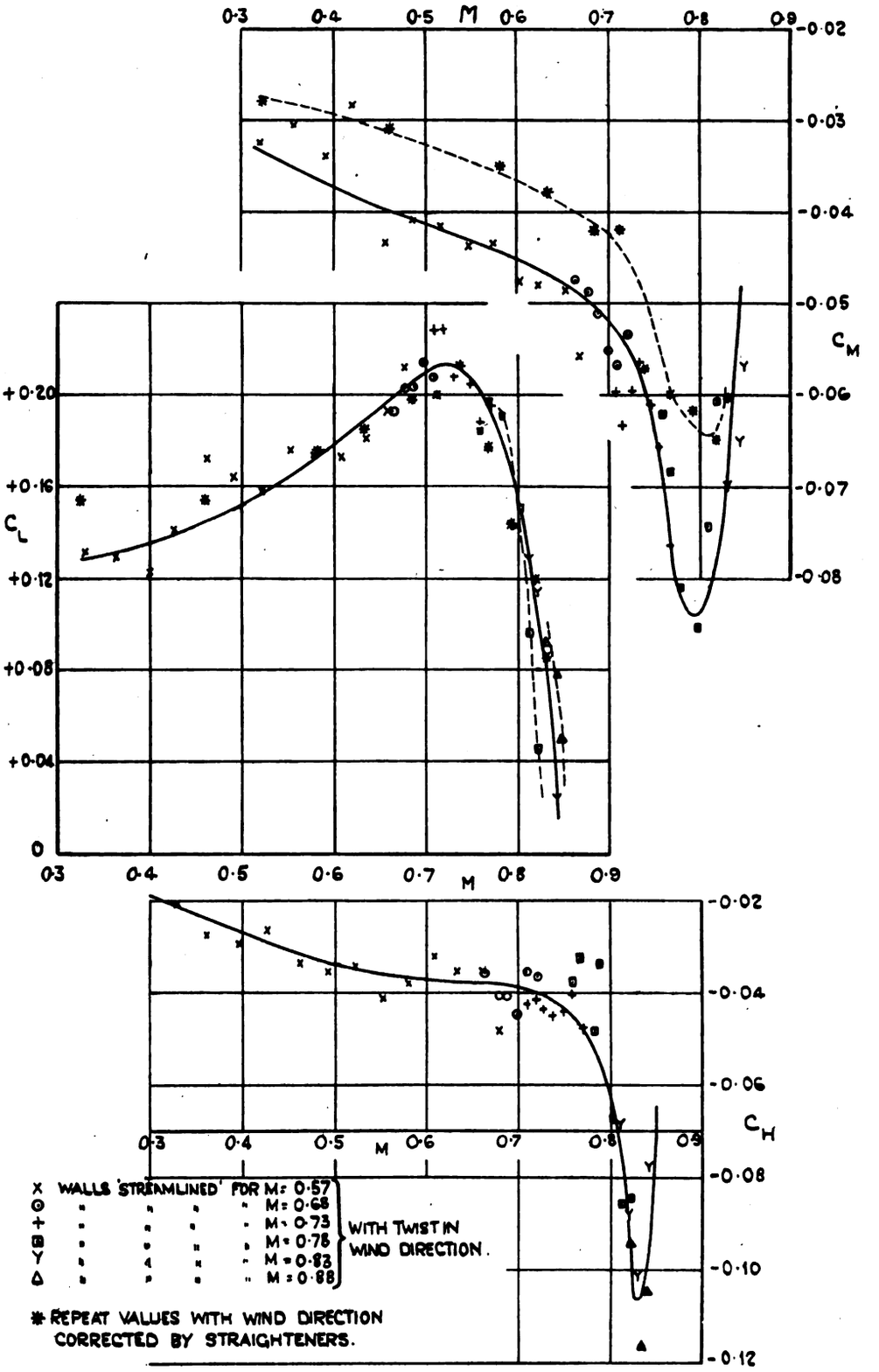

FIG. 38. Integrated Coefficients for $\alpha = 0$ deg. N.P.L. Tests.

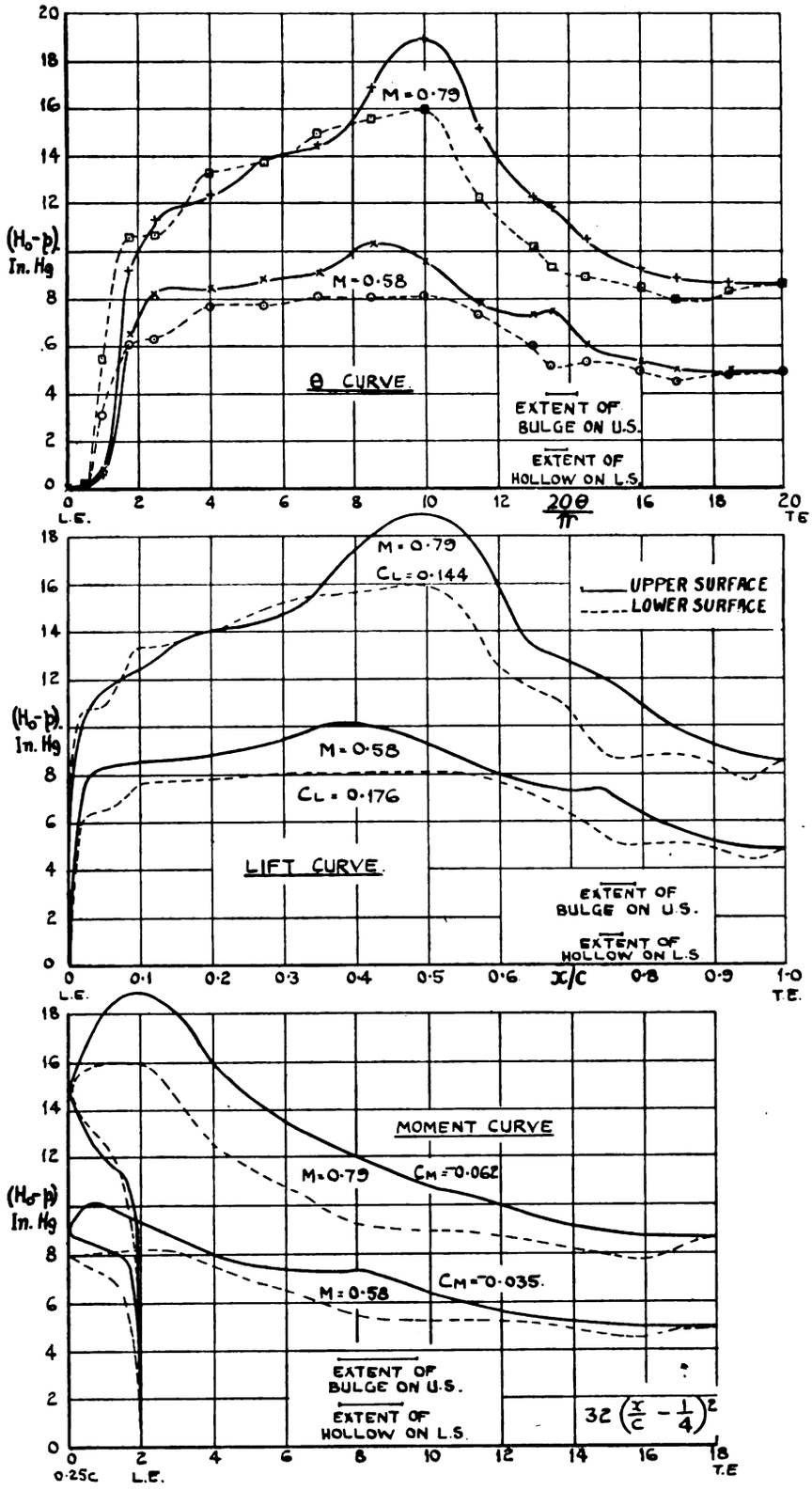

FIG. 39. Reduction of Results. $\alpha = 0$ deg. N.P.L. Tests.

ADDENDUM

Pressure Distribution on a Two-dimensional Mustang Wing Model in the Royal Aircraft Establishment 7-ft. Tunnel*

By

J. S. THOMPSON, B.A. and W. PORT

Summary.—Discrepancies in lift curve slopes measured on a two-dimensional Mustang aerofoil section in the N.P.L. and R.A.E. High Speed Tunnels led to a third series of measurements in the R.A.E. 7-ft. tunnel. These give a lift curve slope greater than that of the R.A.E. High Speed Tunnel, which was itself 10 per cent. greater than the N.P.L. value. The high value in the 7-ft. tunnel is attributed to Reynolds number effects.

1. *Introduction.*—The foregoing report describes measurements of pressure distribution on two-dimensional models of a Mustang wing section in the N.P.L. and R.A.E. High Speed Wind Tunnels. The R.A.E. results gave a lift curve slope about 10 per cent. higher than the N.P.L., even at low Mach numbers. This note describes a third series of pressure plotting tests, which were made on the N.P.L. model in the R.A.E. low-speed 7-ft. tunnel, with the object of clearing up the discrepancy.

2. *Method of Test.*—The model was the 5-inch chord brass aerofoil which had been used for the tests in the N.P.L. High Speed Tunnel. This model had a span of 8 inches, and it was supported in the middle of the R.A.E. 7-ft. tunnel by wooden struts of the same section pinned to its ends. This gave, in effect, a 5-inch chord aerofoil spanning the tunnel vertically, and the pressure plotting holes in the middle four inches of its span.

Pressure differences were measured against a standard hole in the side of the tunnel in the usual way, and were referred to the free stream static by means of the empty tunnel calibration.

Incidences are referred to the geometrical axis of the tunnel, and were measured by reflecting light from a small mirror fixed near the trailing edge of the brass aerofoil. Separate measurements were made to verify that the pressure distribution was not affected by the mirror.

The tunnel speed was 80 ft./sec., giving a Mach number of 0·07 and a Reynolds number of $0{\cdot}2 \times 10^6$.

3. *Presentation of Results.*—The pressure distributions measured at five incidences are given in Fig. 40 in the form C_p plotted against x/c, where C_p is the pressure coefficient $(p - p_0)/\frac{1}{2}\rho V^2$ and x/c is the distance along the chord from the leading edge. Interpolated values for $\alpha = \pm 1$ deg. are compared in Fig. 41 with corresponding curves from the main report.

Values of C_L obtained by integrating the pressure curves are plotted on Fig. 42, together with corresponding points from the main report. The slopes of the mean lines on this figure, with other relevant data, are given in Table 1.

4. *Discussion.*—The differences in the lift curve slopes seem at first sight large, even allowing for some uncertainty in deducing the mean slope from the measured points. The effect of Mach number can be estimated from Glauert's law ($C_L \propto 1/\sqrt{1 - M^2}$), which reduces the values in the two high-speed tunnels by 5 per cent. from $M = 0{\cdot}3$ to $M = 0$. The effect of the large chord/span ratio in the N.P.L. High Speed Tunnel tests is difficult to estimate accurately, but from Ref. 1 it appears that the end effect correction will not increase the slope by more than about 3 per cent.

The values after applying the above corrections are given in the last line of Table 1. The residual differences must be attributed partly to Reynolds number (and turbulence), and partly to experimental inaccuracy. The general effect of Reynolds number is discussed in Ref. 2, to

* R.A.E. Technical Note No. Aero. 1589, February, 1945.

which reference should be made before criticism of these results is attempted, but no precise estimate can be made, particularly for this wing with its bumpy upper surface. The high value of the lift curve slope obtained in the 7-ft. tunnel might possibly be entirely due to the low Reynolds number, but the difference in Reynolds number between the two high-speed tunnels is likely to account only for 1 or 2 per cent. out of the observed difference of 9 per cent. The lift curve slope estimated[3] from the trailing edge angle of 7 deg. is between 0·095 and 0·10 at $R = 10^6$.

There is still a discrepancy of 7 or 8 per cent. between lift curve slopes obtained in the R.A.E. and N.P.L. High Speed Tunnels. This must be taken as an indication of the inconsistency to be expected between tests in the two tunnels, including small differences in model shape and differences in the tunnel flow, as well as experimental errors. Lift curve slope is difficult to measure accurately; it is worth noting that tests on EC 1250 and EQH 1250 quoted in Ref. 2 (Fig. 6) show 50 per cent. change in lift curve slope between $\alpha = 0$ deg. and $\alpha = 3$ deg. at $M = 0{\cdot}6$.

Apart from the slopes of the lift curve, the differences between the results in the 7 ft. and high-speed tunnels are not very serious. The variation in the angles of zero lift in Fig. 42 can be attributed to experimental errors. Neither of the R.A.E. tunnels was calibrated for yaw (the aerofoil was vertical in each case), and in the 7-ft. tunnel the measurement of the datum incidence to the tunnel axis may be in error by 0·2 deg. There are also small differences between the two models which appear in the pressure distributions in Fig. 41, particularly at the nose and at $x/c = 0{\cdot}4$ on the upper surface.

TABLE 1

Tunnel	N.P.L. H.S.T.	R.A.E. H.S.T.	R.A.E. 7 ft.
Aerofoil chord	5 in.	24 in.	5 in.
Aerofoil span	8 in.	84 in.	84 in.
Aerofoil chord/span	0·63	0·29	0·06
Mach number	0·3	0·3	0·07
Reynolds number	$0{\cdot}85 \times 10^6$	$1{\cdot}8 \times 10^6$	$0{\cdot}2 \times 10^6$
Lift curve slope $dC_L/d\alpha$ per degree ..	0·098	0·109	0·115
Lift curve slope corrected to $M = 0$ ..	$0{\cdot}093_5$	0·104	0·115
Lift curve slope corrected for end effects	$0{\cdot}096_5$	0·104	0·115

REFERENCES

No.	Author	Title, etc.
1	J. H. Preston	The Interference on a Wing spanning a Closed Tunnel arising from Boundary Layers on the Side Walls with Special Reference to the Design of Two-dimensional Tunnels. R. & M. 1924. March, 1944.
2	P. R. Owen	Note on the Scale Effect on Stick Fixed Static Longitudinal Stability in the Glide. R.A.E. Technical Note Aero. 1104 (Misc.). A.R.C. 6394. December, 1942. (Unpublished.)
3	C. H. Naylor and D. J. Lyons	An Analysis of the Lifting Characteristics of Aerofoils and Controls with Special Reference to Methods of Estimation for Design Use. R.A.E. Report Aero. 1840. A.R.C. 7149. July, 1943. (Unpublished.)

References to the main report are on page 7.

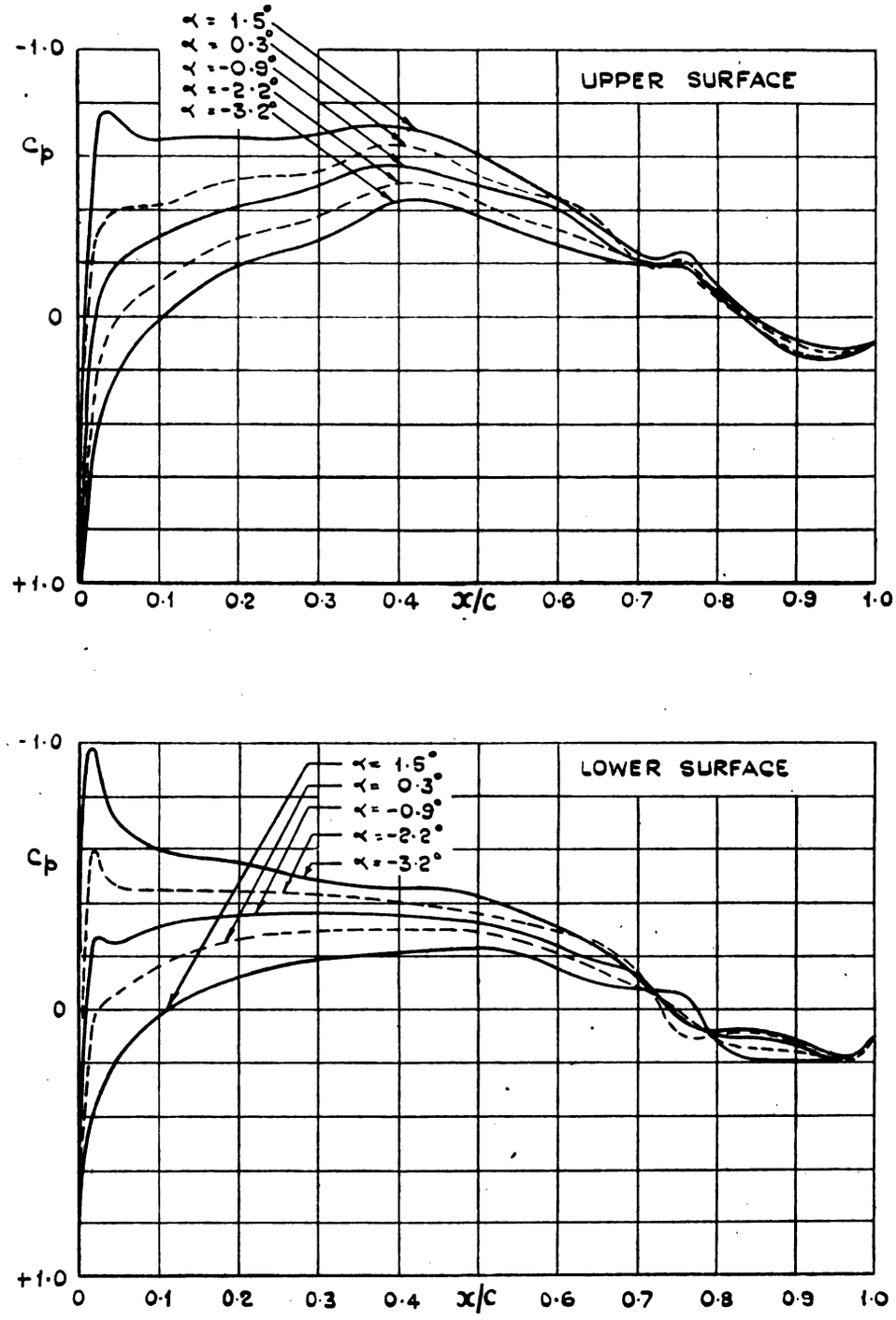

FIG. 40. Pressure Distribution in R.A.E. 7 ft. Tunnel.

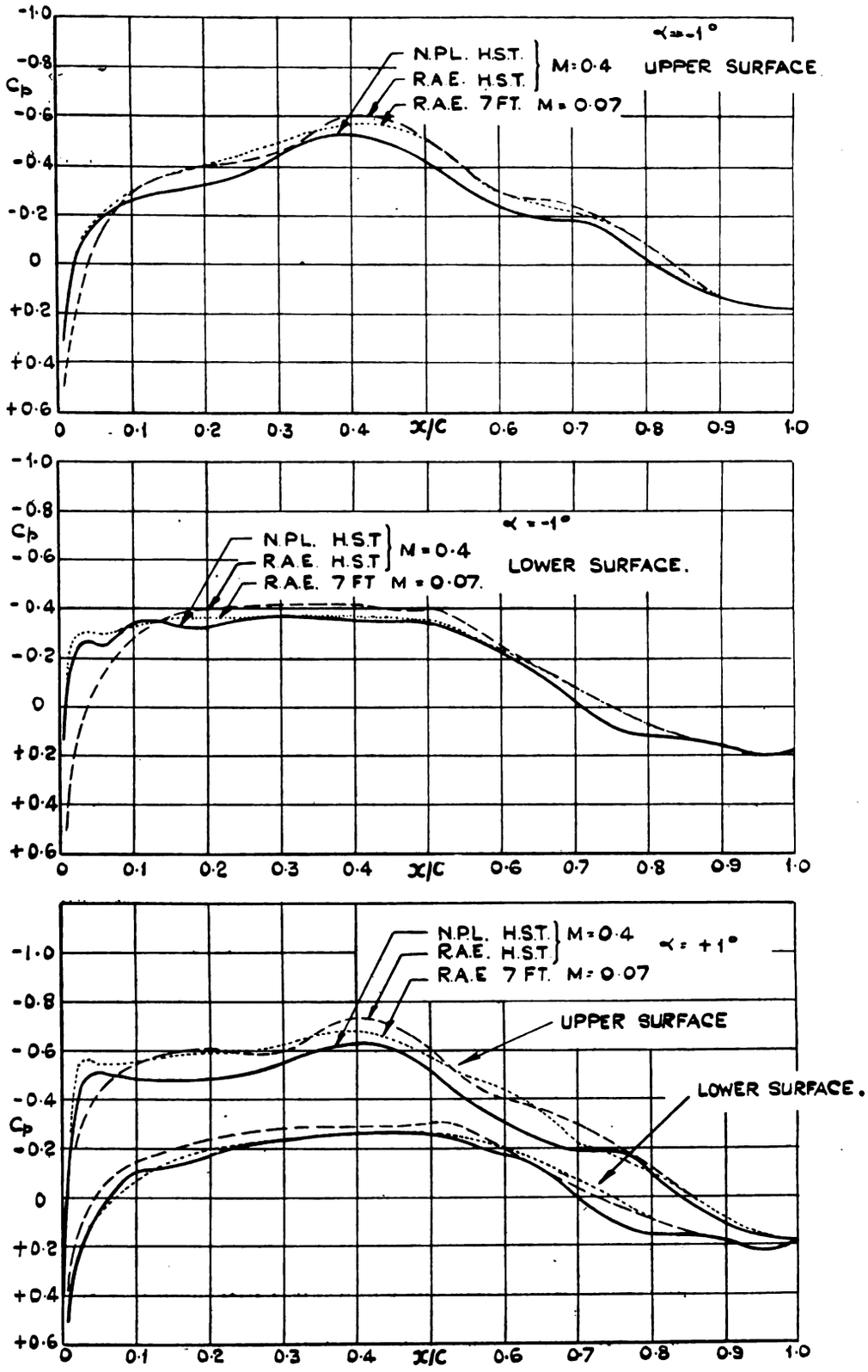

FIG. 41. Pressure Distributions in Various Tunnels.
(*Note.*—The same model was used for N.P.L. H.S.T. tests and R.A.E. 7 ft.)

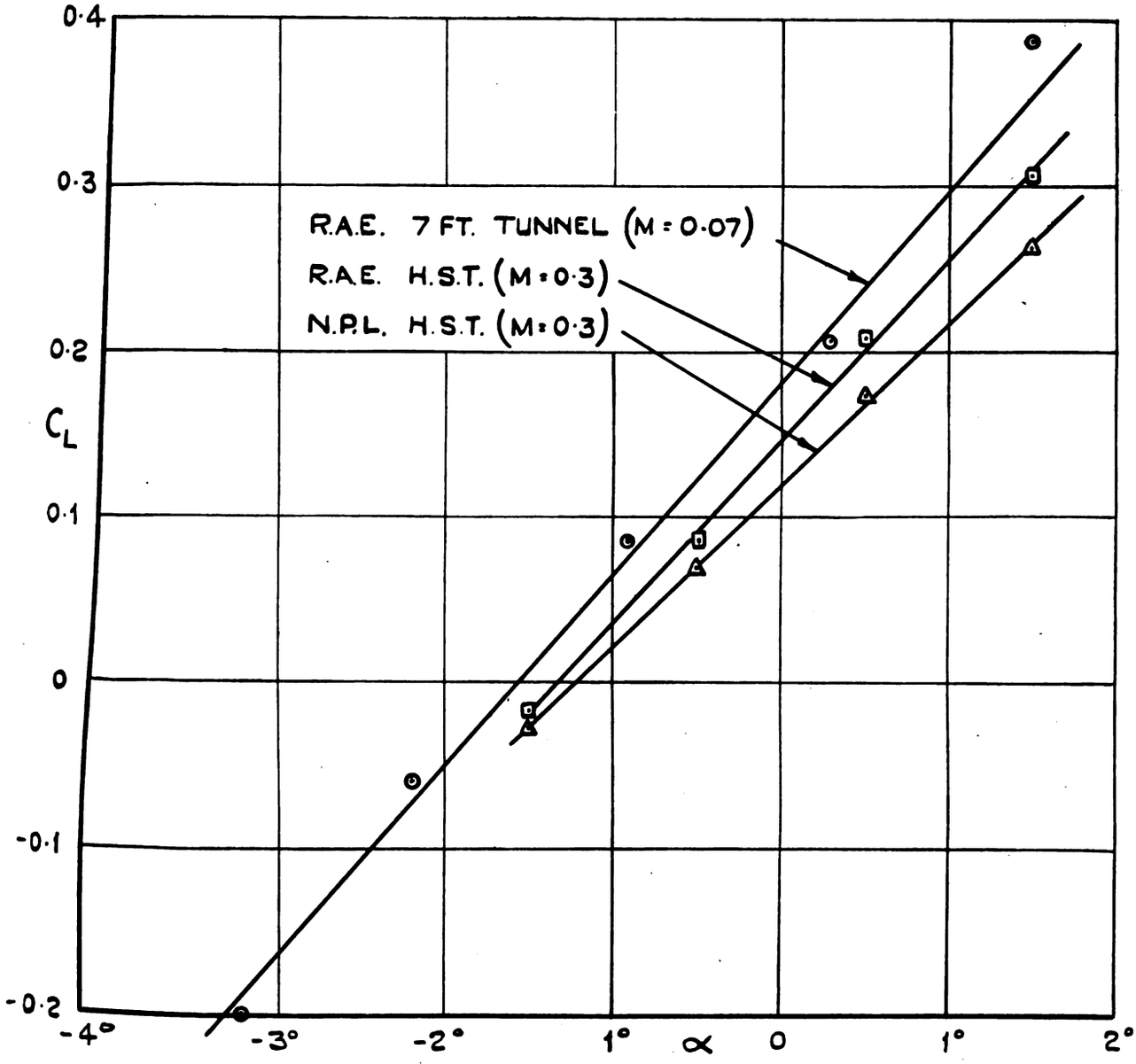

FIG. 42. Lift Curves.

(83488) Wt. 11 6/48 Hw.